THE UNIVERSITY of EDINBURGH

Edinburgh Research Explorer

Volatiles and intraplate magmatism: A variable role for carbonated and altered oceanic lithosphere in ocean island basalt formation

Citation for published version:
Kirstein, L, Walowski, KJ, Jones, RE, Burgess, R, Fitton, JG, De Hoog, C-J, Savov, IP, Kalnins, L & Edinburgh Ion Microprobe Facility, EIMF 2023, 'Volatiles and intraplate magmatism: A variable role for carbonated and altered oceanic lithosphere in ocean island basalt formation', *Journal of Petrology*. https://doi.org/10.1093/petrology/egad022

Digital Object Identifier (DOI):
10.1093/petrology/egad022

Link:
Link to publication record in Edinburgh Research Explorer

Document Version:
Peer reviewed version

Published In:
Journal of Petrology

Publisher Rights Statement:
© The Author(s) 2023. Published by Oxford University Press.

General rights
Copyright for the publications made accessible via the Edinburgh Research Explorer is retained by the author(s) and / or other copyright owners and it is a condition of accessing these publications that users recognise and abide by the legal requirements associated with these rights.

Take down policy
The University of Edinburgh has made every reasonable effort to ensure that Edinburgh Research Explorer content complies with UK legislation. If you believe that the public display of this file breaches copyright please contact openaccess@ed.ac.uk providing details, and we will remove access to the work immediately and investigate your claim.

OPEN ACCESS

Download date: 02. May. 2023

Volatiles and intraplate magmatism: A variable role for carbonated and altered oceanic lithosphere in ocean island basalt formation

Linda A. Kirstein[1]*, Kristina J. Walowski[2], Rosemary E. Jones[3], Ray Burgess[4], J. Godfrey Fitton[1], Jan C.M. De Hoog[1], Ivan P. Savov[5], Lara A. Kalnins[1], EIMF[6]

1 University of Edinburgh, School of GeoSciences, Grant Institute, Edinburgh, UK

2 Western Washington University, Department of Geology, Bellingham WA, USA

3 University of Oxford, Department of Earth Sciences, Oxford, UK

4 University of Manchester, Department of Earth and Environmental Sciences, Manchester UK

5 University of Leeds, School of Earth and Environment, Leeds, UK

6 Edinburgh Ion Microprobe Facility, Grant Institute, University of Edinburgh, Edinburgh, UK

*Corresponding Author

Contact Information: linda.kirstein@ed.ac.uk

Abstract

Recycling of material at subduction zones has fundamental implications for melt composition and mantle rheology. Ocean island basalts sample parts of the mantle from variable depths that have been diversely affected by subduction zone processes and materials, including the subducted slab, metasomatising melts and fluids. Resultant geochemical differences are preserved at a variety of scales from melt inclusions to whole rocks, from individual islands to chains of islands. Here we examine a global dataset of ocean island basalt compositions with a view to understanding the connection between silica-saturation, olivine compositions, and halogens in glass and olivine-hosted melt inclusions to reveal information regarding the mantle sources of intraplate magmatism. We find that minor elements incorporated into olivine, although informative, cannot unambiguously discriminate between different source contributions, but indicate that none of the OIB analysed here are derived solely from dry peridotite melting. Nor can differences in lithospheric thickness explain trace element variability in olivine between different ocean islands. We present new halogen (F, Cl, Br/Cl, I/Cl) data along with incompatible trace element data for the global array and encourage measurement of fluorine along with heavier halogens to obtain better insight into halogen cycling. We suggest that Ti-rich silica-undersaturated melts require a contribution from carbonated lithosphere, either peridotite or eclogite and are an important component sampled by ocean island basalts, together with altered oceanic crust. These results provide new insights into our understanding of mantle-scale geochemical cycles, and also lead to the potential for the mantle transition zone as an underestimated source for observed volatile and trace-element enrichment in ocean island basalts.

© The Author(s) 2023. Published by Oxford University Press. This is an Open Access article distributed under the terms of the Creative Commons Attribution License https://creativecommons.org/licenses/by/4.0/, which permits unrestricted reuse, distribution, and reproduction in any medium, provided the original work is properly cited.

ORIGINAL UNEDITED MANUSCRIPT

Downloaded from https://academic.oup.com/petrology/advance-article/doi/10.1093/petrology/egad022/7115969 by University of Edinburgh user on 18 April 2023

INTRODUCTION

The presence of volatiles (e.g. H_2O, CO_2, halogens) in nominally volatile-free minerals in the mantle has significant implications for mantle rheology, melt generation and the Earth's deep volatile cycle (e.g. Giacomoni et al., 2020; Kirstein et al., 2001). Intraplate ocean island basalts (OIB) are enriched in incompatible trace elements compared with those at mid-ocean ridges (MOR). The extent of enrichment of volatile elements may be a key driver for generating some of the geochemical heterogeneity measured in erupted magmas. This heterogeneity is observed in OIB globally and varies between island groups (e.g. Galapagos vs. Samoa; Gazel et al., 2018; Mundl et al., 2017), islands in the same volcanic chain (e.g. Pitcairn; Woodhead & McCulloch, 1989), and in some cases, within a single island (e.g. Kilauea, Hawai'i; Garcia et al., 2016). Numerous geochemical investigations of OIB indicate that this is partly a reflection of differences in depth and degree of melting and partly generated by recycling, multistage melting and metasomatism (e.g. Dixon et al., 2017) over Earth's history.

Subduction leads to the recycling of tectonic plates into the mantle. Due to differences in density and mechanical strength, some subducting slabs (including the deeply subducted serpentinite component (Smith et al., 2021)) stagnate in the mantle transition zone (MTZ), while others penetrate into the lower mantle. The mantle transition zone located between ~410 and ~660 km depth has been proposed as a store of incompatible and volatile elements based on the discovery of ringwoodite inclusions in diamond (Pearson et al., 2014) and is a potential source of intraplate magmatism (Kuritani et al., 2019; Mazza et al., 2019). Geodynamic processes, as well as mineralogical phase changes, make the transition zone both enriched and heterogeneous. The MTZ is a region that lower mantle plumes must pass through *en route* to the surface.

Major-, trace- and volatile-element chemistry of minerals, glass and melt inclusions can be useful in distinguishing between different source compositions. The mantle, although predominantly composed of peridotite, also contains recycled oceanic lithosphere in the form of eclogite produced by high-pressure metamorphism of mafic crust, and pyroxenite formed by reaction of peridotite with silicic partial melt from eclogite (van Acken et al., 2010). Infiltration of mantle peridotites by low-degree melts that are enriched in volatile- and incompatible elements could induce variations in mantle mineralogy (e.g. metasomatic minerals, veining). Carbonate-rich silicate melts, formed by reaction between CO_2 and clinopyroxene, are also present in lherzolite where temperature and pressure conditions allow (Ionov, 1998). Such melts will percolate upwards and enrich the lithosphere-asthenosphere boundary zone (e.g. Guimarães et al., 2020). The combination of all these processes results in a mantle that is highly heterogeneous over a variety of temporal and spatial scales.

The degree of silica saturation in mafic igneous rocks is a useful proxy for depth and degree of melting and can be quantified through the silica saturation index (SSI = 100 (Si - (Al+Fe^{2+}+Mg+3Ca+11Na+11K+Mn-Fe^{3+}-Ti-10P)/2), where Si etc. are the molecular proportions of the respective oxides (Gill and Fitton, 2022). SSI is based on the CIPW norm, and reflects the excess or deficiency of silica with respect to a standard mineral assemblage (olivine, clinopyroxene and plagioclase) that defines the critical plane of silica-undersaturation (Yoder and Tilley, 1962). Deep, small degrees of melting will produce alkali-rich, silica-undersaturated basaltic magmas, while silica-saturated basaltic magmas will result from large degrees of melting at lower pressure. When melted, pyroxenite produces silica-saturated to oversaturated liquids (Sobolev et al., 2007). Similarly, partial melting of eclogite will also produce silica-saturated liquids. The incorporation of carbonate-rich melt into small-degree silicate melts will increase the degree of silica-undersaturation (Gill and Fitton, 2022) and alter the liquidus phase volume of olivine (Herzberg, 2011). SSI can therefore provide a first-order indication of source composition and degree and depth of melting, while volatile elements including the halogens can provide important information on recycling as they are a major constituent of the oceans.

The use of halogens to date, however, has been limited by the scarcity of data from OIB. Major-, trace-element and isotope ratios indicate large variability in source compositions, depth and degree of melting across a range

ORIGINAL UNEDITED MANUSCRIPT

Downloaded from https://academic.oup.com/petrology/advance-article/doi/10.1093/petrology/egad022/7115969 by University of Edinburgh user on 18 April 2023

of OIB but such studies rarely consider the potentially important role that variable volatile contents, particularly the halogens, play in controlling melt generation. Here, we use olivine composition, silica-saturation and halogen concentrations in melt inclusions and glass from a global OIB dataset to reveal information regarding the mantle sources of intraplate magmatism. New data along with previously published data (Walowski et al., 2021) are presented from a suite of subaerial tephra and submarine basalts from eight ocean islands including La Palma (Canary Islands), Fogo (Cape Verde), St. Helena, Ascension Island, Tristan da Cunha, MacDonald (Ra) Seamount, Pitcairn Islands and La Réunion (Figure 1). These data are compared to published data from other ocean islands, including Hawai'i (Sobolev et al., 2007; Dixon et al., 2008; Sisson et al., 2009), El Hierro (Canary Islands) (Taracsák et al., 2019), Iceland (Spice et al., 2015; Hartley et al., 2021) and the Cook Islands (Mangaia, Tuvalu, Karthala; Cabral et al., 2014; Weiss et al., 2016; Hanyu et al., 2019) for a more complete global comparison that samples the entire range of OIB composition.

TRACE ELEMENTS IN OLIVINE

Olivine compositions reflect the mantle source(s) of the melt from which they crystallise and are affected by temperature- and pressure-dependent mineral-melt partition coefficients (Sobolev et al., 2007; de Hoog et al., 2010; Herzberg, 2011; Matzen et al., 2013; Gavilenko et al., 2016; Matzen et al., 2017). Olivine crystallises over a range of pressures in basaltic magmas and contains a number of minor/trace elements including Al, Ni, Mn and Ca that can be used as possible petrogenetic indicators (e.g. de Hoog et al., 2010). Calcium, along with Al, is moderately incompatible in olivine; as a result, low-degree partial melts of peridotite are enriched in CaO (>~10 wt.%) with Ca_{ol} >1500 ppm (Herzberg, 2011). Calcium in olivine (Ca_{ol}) is also influenced by magmatic H_2O content, but not temperature (Gavrilenko et al., 2016), while Al-in-olivine is a well-known geothermometer due to its temperature-sensitive partitioning behaviour (e.g. Spice et al., 2016). Nickel partitioning has recently been shown to be temperature- and pressure-sensitive (Matzen et al., 2013; Matzen et al., 2017), while Mn partitioning into olivine is influenced by pressure and the presence of garnet (Matzen et al., 2017).

Low-degree partial melts of silica-rich pyroxenite are often low in CaO due to the effect of residual clinopyroxene, but some pyroxenites may be high in CaO, having formed as cumulates deep in the mantle (Herzberg, 2011). Partial melts of pyroxenite can be higher in FeO/MnO than partial melts of peridotite due to phase compositional differences (Herzberg, 2011). Melt fraction also influences Fe/Mn_{ol} with high FeO/MnO (>80) indicative of low pyroxenite partial melt fractions at 2-3.5 GPa (Herzberg, 2011).

Here we focus on elemental abundances (Mn, Ni, Al, Ca and Fe) that can be measured by electron-probe micro-analysis (EPMA) to explore whether it is possible to discriminate melting of peridotite and/or pyroxenite source components, cognisant of the control that variable temperature, pressure and volatile contents may have on olivine composition (Herzberg, 2011; Matzen et al., 2017). The relationship between Ni and Mn and lithospheric thickness is also examined.

HALOGENS IN THE MANTLE

Estimates of halogen degassing fractions from the present-day mantle vary but are typically up to ~46-88% for the most degassed elements Br and I (e.g., Kendrick et al., 2017; Guo and Korenaga, 2021). Surface halogens (Cl, Br and I) are primarily concentrated in ocean water and marine sediments so should act as ideal tracers of subduction cycling (e.g. John et al., 2011; Kendrick et al., 2017; Broadley et al., 2018; Kendrick and Barnes, 2022). Recycling at subduction zones effectively fractionates fluid-mobile from less-mobile elements with phase changes also controlling partitioning behaviour (e.g. Jones et al., 2014; Debret et al., 2016; Urann et al., 2017). The mantle wedge above the subducting slab is enriched in mobile elements including chlorine and fluorine through percolation of slab-derived aqueous fluids (Cl) (John et al., 2011) and silicate melts (F) (Wu and Koga, 2013), and over time may chemically exchange with the rest of the upper mantle. Sub-critical aqueous fluids have remarkably little carrying capacity for incompatible trace elements, unlike supercritical

ORIGINAL UNEDITED MANUSCRIPT

Downloaded from https://academic.oup.com/petrology/advance-article/doi/10.1093/petrology/egad022/7115969 by University of Edinburgh user on 18 April 2023

fluids and silicate melt (Ni et al., 2017). The water and halogen contents of the upper mantle are different to primitive mantle and reflect the subduction of serpentinised lithospheric mantle and altered oceanic crust (AOC) (Kendrick et al., 2017).

Chlorine is a major component of seawater and is enriched in altered oceanic lithosphere, while fluorine and iodine are preferentially incorporated into naturally occurring polymorphs of calcium carbonate (Feng et al., 2021). Marine carbonates and clay minerals can contain significant amounts of F preserved in sediments that can only be mobilised during high-grade metamorphism (Kendrick and Barnes, 2022). Seafloor serpentinites can also have notably high concentrations of halogens, higher than normal eclogite (Kendrick and Barnes, 2022). Altered oceanic crust (AOC) is strongly enriched in Cl, Br, and I while the lack of F enrichment can be explained by the low solubility of F in seawater (Kendrick and Barnes, 2022). Contamination of the mantle by AOC is clearly demonstrated for the HIMU reservoir (e.g. Cook Islands) but less so for enriched mantle (Pitcairn, Samoa) where metasomatic enrichment and sediments have been invoked (Cabral et al., 2014; Weiss et al., 2016; Kendrick et al., 2017; Hanyu et al., 2019). Although halogens are incompatible during melting of mantle peridotite, fluorine is significantly more compatible than H_2O, while chlorine is significantly less compatible. Global MORB compositions contain ~ 170 ppm F (Arevala and McDonough, 2010), with average depleted and enriched MORB-source mantle containing 8 and 31 ppm F, respectively (Shimizu et al., 2016). Fluorine in oceanic peridotites is mostly hosted in pyroxene and olivine (Urann et al., 2017), which suggests pyroxenites could host significant amounts of F. Eclogitized oceanic crust can host more F and Cl than can depleted oceanic (harzburgitic) mantle which is clinopyroxene-poor. Fluorine is also trapped in the down-going slab in mineral phases such as serpentine, apatite, phengite, titanite and amphibole (Debret et al., 2013; Page et al., 2016; Urann et al., 2017) and partitions into omphacite during eclogite formation (Debret et al., 2013). Amphibole will preferentially incorporate F^- and Cl^- over Br^- and I^-. In summary, F is preferentially retained in the mantle and continental crust (Kendrick et al., 2017), with anhydrous peridotite mantle containing 1.4-31 ppm F (Urann et al., 2017). Due to the differences in compatibility between F and the heavier halogens, altered ocean crust is less enriched in F than Cl, Br and I.

Chlorine is volatile, is incompatible during silicate melting and is water soluble (Cl-rich materials include seawater, brines and altered rocks) with concentrations of <1 ppm in peridotitic mantle (Bonifacie et al., 2008; Urann et al., 2017). It is therefore ideal for tracing seawater-derived volatiles in recycled materials at subduction zones and in the mantle. Chlorine concentrations in MORB are variable, extending to ~140 ppm (Arevala and McDonough, 2010), with MORB-source mantle containing 0.4 to 22 ppm Cl (Shimizu et al., 2016). There is evidence of recycling of Cl into the lower mantle, with melt inclusions from the Austral-Cook islands showing high Cl (up to 1500 ppm) associated with radiogenic lead ($^{207}Pb/^{206}Pb$ >0.75) thought to indicate ancient subducted oceanic crust (Hanyu et al., 2019). Melting of halogen-rich lithologies can enrich OIB in halogens, although high quality data on the halogen content of OIB are currently limited. During partial melting, Cl has similar incompatibility to K and Nb so ratios such as Cl/K and Cl/Nb should reflect source characteristics (Hanyu et al., 2019), if assimilation processes are minor (e.g. Kendrick et al., 2017). Similarly, ratios of volatile to non-volatile trace elements that have similar mineral-melt partitioning during melting e.g. F/Zr, F/ Pr and H_2O/Ce (Cabral et al., 2014), can provide insights into enrichment processes but may show covariations from fractionation during subduction-related processes (e.g. Kendrick et al., 2017).

The heavier halogens, Br and I, when ratioed to Cl are highly useful for discriminating between primary source signatures and different contamination processes as they are fractionated in surface reservoirs and seafloor settings (Kendrick and Barnes, 2022). For example, seawater has a low I/Cl ratio (Kendrick, 2018), while high I/Cl in basaltic glass can be attributed to palagonite formation (Kendrick et al., 2012). These ratios, when coupled with other tracers are useful in distinguishing the role of serpentinites and AOC (Snyder et al., 2004; Chavrit et al., 2016). High Br/Cl and I/Cl is indicative of marine pore fluids or brine assimilation (Sumino et al., 2010; Broadley et al., 2016).

ORIGINAL UNEDITED MANUSCRIPT

Downloaded from https://academic.oup.com/petrology/advance-article/doi/10.1093/petrology/egad022/7115969 by University of Edinburgh user on 18 April 2023

Here we track some of the recycled components using volatile elements, including the halogens, to draw conclusions on where and how OIB obtain some of their distinctive geochemical signatures. Despite the potential for heterogeneity, many OIB are remarkably geochemically uniform. For example, recent studies on the $\delta^{11}B$ composition of OIB show little global variability, with a range from -12 to -5‰ (Walowski et al., 2019; 2021) which suggests that signatures of recycling (if originally present) may be diluted over time. Alternatively local serpentinisation of olivine-rich rocks in the lithosphere may be an important contributor of halogens and other volatiles (e.g. Kendrick and Barnes, 2022).

SAMPLES

Samples were acquired from eight ocean islands including La Palma (Canary Islands), St. Helena, Fogo (Cape Verde), Ascension Island, Tristan da Cunha, MacDonald (Ra) Seamount, Pitcairn Islands and La Réunion (Table 1). They have previously been described by Walowski et al. (2019, 2021), and so only a summary table is provided here (Table 1).

The xenolith samples from La Palma are dunites, consisting primarily of olivine (Fo = 80.5), with minor amounts of clino- and orthopyroxene, and accessory chrome spinel. These ultramafic xenoliths were present in sequences of basaltic lava flows (~0.7 Ma) in the Barranco Fagundo.

We compare our olivine, melt inclusion and glass data with selected published datasets. Olivine compositions are compared with Hawai'i (Hammar et al., 2006; Dixon et al., 2008; Sisson et al., 2009; Garcia et al., 2016); Iceland (Hartley et al., 2021); Canary Island (El Hierro) (Taracsák et al., 2019); Greenland; North Atlantic igneous province (Spice et al. 2015) and the Cook Islands (Mangaia, Tuvalu, Karthala; Cabral et al., 2014; Weiss et al., 2016; Hanyu et al., 2019). Melt inclusions and glass are compared with Cook-Austral HIMU islands (Hanyu et al., 2019) and Hawai'i (Sisson et al., 2009). Finally, published halogen data from diamonds are from Johnson et al. (2000) and Burgess et al. (2002). The aim is to resolve differences in composition and specifically the impact of volatile-rich components on OIB composition.

METHODS

All samples analysed in this study were collected from subaerial or submarine deposits including coarse-ash size fraction of tephra deposits and glass shards. Individual loose olivine phenocrysts (250 µm to 2 mm in length) and glass fragments were hand-picked from sieved material and examined in immersion oils or alcohol to locate the melt inclusions. For each sample, epoxy resin mounts were made with individual submarine glass shards, and olivine-hosted melt inclusions together with standards. The epoxy mounts were polished, cleaned and coated in Au. Volatile (Cl and F) and selected trace elements (Rb, Sr, Y, Zr, Nb, Ba, La, and Ce) were analysed in the same mounts using a Cameca IMS-4f secondary ion mass spectrometer at the NERC Edinburgh Ion Microprobe Facility (EIMF). Data for this study were collected in two separate analytical sessions using identical setups (Walowski et al., 2019; Walowski et al., 2021). Analyses were made using a primary beam of $^{16}O^-$ ions with a net impact energy of 14.5 keV and a beam current of 5 nA, resulting in a spot size of ~20µm at the sample surface. During SIMS analysis positive secondary ions were extracted at 4425 V using an energy window of ±25 eV. The trace element analyses were done using a mass resolution of 300 (M/ΔM). The following mass stations were measured (total counting times for each in brackets, divided into 6 cycles): ^{1}H (30s), ^{7}Li (30s), ^{11}B (60s), ^{19}F (60s), ^{26}Mg (12s), ^{30}Si (12s), ^{35}Cl (60s), ^{39}K (18s), ^{47}Ti (30s), ^{84}Sr (30s), ^{85}Rb (30s), ^{88}Sr (30s), ^{89}Y (30s), ^{90}Zr (30s), ^{93}Nb (30s), ^{138}Ba (30s), ^{139}La (30s), ^{140}Ce (30s). For listed trace elements, the instrumental background was considered to be negligible with the exception of H. ^{85}Rb was corrected for FeSi molecular interference based on the ^{84}Sr signal (which is dominantly $^{28}Si^{56}Fe$ after subtraction of true ^{84}Sr based on the ^{88}Sr signal). GSD1-G was used as a calibration standard for trace elements, and BCR2-G, ATHO-G, T1-G, StHs-G, KL2-G as secondary standards (GeoReM Preferred Values, Jochum and Stoll, 2008). Additional standards specifically for Cl and F analyses included StA (Lesne et al. 2011), Lipari (Jochum and Stoll, 2008) and

ORIGINAL UNEDITED MANUSCRIPT

Downloaded from https://academic.oup.com/petrology/advance-article/doi/10.1093/petrology/egad022/7115969 by University of Edinburgh user on 18 April 2023

Fba (Guggino & Hervig, 2010). Supplementary file A contains all measurements of standard materials. Uncertainty for the analyses of Li, B, Cl and F is 5% based on the highest concentration standard (S4-13, n=5), which fall within the range of concentrations measured.

The following standards were used for electron probe calibration: jadeite for Na, spinel for Mg and Al, orthoclase for K, wollastonite for Si and Ca, synthetic fayalite for Fe, Durango apatite for P, rutile for Ti, and pure metals for Mn, Cr and Ni. Cameca software, PeakSight, was used to process data after collection, and analyses with poor totals (outside of the range 97-101%), were not included in the final dataset. Elements were analyzed in the following order: Na, Mg, Al, Si, K, K, Ca, Fe, Ca, P, Ti, Mn, P, Ti. Three sigma standard deviation was <0.1 wt.% for Mg, K, Mn, Cl, P, S, Ti, F; <0.3 wt.% for Al, Ca, Fe; <0.5 wt.% for Na and <1 wt.% for Si. Glass standards BCR2, VG2, VG-A99 were run at University of Bristol. See Supplementary file A for all analyses.

The mounts containing the glasses and olivine-hosted melt inclusions were carbon coated and analysed for major elements, minor elements and volatiles (F, Cl) on the Cameca SX-100 electron microprobe at the University of Edinburgh and at the University of Bristol (UoB). Analyses were performed using a 5 µm beam and an accelerating voltage of 15 kV. A low beam current of 1 nA was used as an added precaution against Na mobilisation in the melt inclusions and glasses. An excellent correlation between MgO from electron microprobe and SIMS trace element routines was found, indicating minimal contribution from the olivine host.

Halogens (Cl, Br, I) were analysed by the neutron-irradiation noble gas mass spectrometry (NI-NGMS) method (Kendrick, 2012; Ruzié-Hamilton et al. 2016; Kobayashi et al., 2021). Neutron irradiation of samples produces proxy noble gas isotopes: $^{38}Ar_{Cl}$, $^{39}Ar_{K}$, $^{80, 82}Kr_{Br}$ and $^{128}Xe_{I}$ which are either absent from, or have low natural abundances in air. This enables the determination of ppm-ppb concentrations of halogens in mg-sized sample aliquots. Note that we do not report any natural noble gas isotope abundances or ratios in this study. Mineral separates of olivine and/or fresh glass fragments were hand-picked under a binocular microscope from lightly crushed bulk samples. The olivine separates and glass were ultrasonically cleaned in ethanol and deionised water to remove adhering particles and dried in an oven heated to 40°C. Approximately 15-50 mg aliquots were wrapped in aluminium foil and sealed in evacuated quartz tubes for neutron irradiation. Standard minerals were spaced throughout the tubes to monitor neutron conversion of K, Cl, Br and I: Hb3Gr to monitor Cl, K (via the J value; Roddick, 1983); Shallowater meteorite to monitor the production of I (Brazzle et al., 1999); scapolite mineral standards to monitor production from Br (Kendrick, 2012); and K- and Ca-doped, Ar-free glass to monitor minor interfering Ar species derived from potassium and calcium. Samples were irradiated in 2018: irradiation designated MN2018a contained samples from all locations. Irradiation was for 24 hours in the flooded reflector area of the Missouri University Research Reactor (MURR), Columbia, Missouri, USA in April 2018 (MN2018a) with fast and thermal neutron fluences of 0.3×10^{18} n cm^{-2} and 4.2×10^{18} n cm^{-2} respectively. Combined monitor data for all tubes irradiated in the same sample container were used to account for minor vertical variations in neutron flux. Lagrange interpolation method was used to fit a polynomial to the monitor data to interpolate noble-gas-element conversion factors for each sample based on their known positions in the tube. Further details of the relevant irradiation parameters are summarised in Supplementary file A.

Proxy noble gas isotope abundances were determined on a Thermofisher Scientific ARGUS VI multi-collector noble gas mass spectrometer at the University of Manchester. Following irradiation, 5-15 mg aliquots of each sample were loaded into 3mm holes drilled into an aluminium sample holder and placed into a laser port. Duplicates of most samples were analysed to check for consistent results. During evacuation, samples were heated at ~120°C for at least 12 hours to remove adsorbed atmospheric gases and achieve UHV. Gases were extracted from samples using a Photon Machines 55W CO_2 fusion laser, with a 3 mm diameter defocused beam using output powers of up to 40 W for up to 130 s to achieve fusion. The released gases were purified for 5 minutes by exposure to two SEAS NP10 Zr-Al getters at room temperature and approximately 300°C,

ORIGINAL UNEDITED MANUSCRIPT

Downloaded from https://academic.oup.com/petrology/advance-article/doi/10.1093/petrology/egad022/7115969 by University of Edinburgh user on 18 April 2023

respectively, and the purified noble gases were then expanded into the mass spectrometer. Throughout the analytical period, blanks were determined either before every, or every other sample analysis depending on blank stability. A calibrated aliquot of air was measured daily for Ar, Kr and Xe isotopes in order to monitor instrument performance, mass discrimination and sensitivity.

Raw data were regressed according to an exponential asymptotic model to time zero (corresponding to gas inlet), except where the exponential model provided a poor fit to the raw data, in which case a linear model was used. Data were corrected for blank contributions, minor instrumental mass-discrimination on Ar, and the instrument sensitivity. Minor corrections were made for radioactive decay of unstable species (^{37}Ar, ^{39}Ar), interfering irradiation-produced species ($^{40}Ar_K$, $^{39}Ar_{Ca}$, $^{38}Ar_K$, $^{36}Ar_{Ca}$, $^{84}Kr_U$) and decay of $^{38}Ar_{Cl}$ on ^{36}Ar (Ruzié-Hamilton et al. 2016). Any atmospheric contribution on ^{40}Ar, $^{38}Ar_{Cl}$, $^{80}Kr_{Br}$ or $^{128}Xe_I$ was subtracted by normalising to the non-radiogenic isotopes ^{36}Ar, ^{84}Kr and ^{132}Xe using their isotopic ratios in air. The effects of these corrections were mostly <10%, <1% and <5% for $^{38}Ar_{Cl}$, $^{80}Kr_{Br}$ and $^{128}Xe_I$, respectively. Typical blanks were low relative to total sample release with typical corrections being <2% $^{38}Ar_{Cl}$, <1 % $^{80}Kr_{Br}$ and < 2% $^{128}Xe_I$. Unless otherwise stated, halogen and K abundance ratios are given as wt./wt. and their concentrations as weight %, ppm or ppb as appropriate; noble gas abundance ratios are reported as mol/mol and concentrations as cm^3/g at standard temperature and pressure (STP). All values are quoted to 1 standard deviation, unless otherwise stated. All data are reported in Supplementary file A.

The major element compositions of individual melt inclusions were corrected for post entrapment crystallization (PEC) using Petrolog 3.1.1.3 (Danyushevsky and Plechov, 2011) with the same conditions as those used by Walowski et al. (2021). Concentrations of trace elements that are incompatible in the olivine hosts were corrected using the Petrolog results assuming similar behaviour to K_2O during PEC. Glass and melt inclusion data from the same samples were compared to estimate potential loss of volatiles in subaerially erupted glasses. All glass analyses are likely to represent minimum values.

All lithospheric thicknesses were extracted using LITHO1.0 a 1° tessellated model of the crust and upper mantle (Pasyanos et al., 2014).

RESULTS

Olivine composition

The analysed olivines from La Réunion, Pitcairn, La Palma, Fogo, MacDonald and Ascension are phenocrystic and not mantle-derived xenocrysts, as evidenced by their elevated Ca, Mn and Al contents (relative to residual/mantle olivine). Average major- and trace-element data from measurements of olivine are presented in Table 2 and full data in Supplementary file A. Olivine compositions in the different OIB samples have a range in forsterite (Fo = atomic Mg/(Mg+Fe)*100) from Fo_{73} to Fo_{87} (Figure 2), lower than mantle values (Fo>89). Olivine compositions between the various OIB samples are distinguishable. La Réunion olivine is the most primitive with the highest Fo and Ni, and relatively low Ca contents (Figure 2). The Pitcairn olivine, from two different volcanoes (Volcano 2 and Volcano 5), varies in composition; Volcano 2 olivine tends to have higher Fo, Ca, Mn/Fe and lower Al compared to Volcano 5 olivine (Figure 2). These olivine populations have different compositions to olivine from both La Palma and La Réunion with the same Fo range. Volcano 5 olivines have higher Ni and lower Mn/Fe than both La Palma and Fogo olivines with the same Fo content (Figure 2). The olivine from Ascension is relatively evolved (Fo = 73). Average Ca contents also vary among OIB samples, ranging from 1484 ppm (La Réunion) to 2206 ppm (Fogo).

All olivine compositional data were regressed to an Mg# of 87, the most primitive olivine composition analysed, to remove the potential effects of fractionation on the oxide composition, and the relationship between NiO_{87} and MnO_{87} was examined (Figure 2).

ORIGINAL UNEDITED MANUSCRIPT

Downloaded from https://academic.oup.com/petrology/advance-article/doi/10.1093/petrology/egad022/7115969 by University of Edinburgh user on 18 April 2023

Halogen data from olivine separates from Fogo, La Palma, Pitcairn, MacDonald, Iceland and La Réunion, were collected using neutron-irradiation noble gas mass spectrometry (NI-NGMS). The majority of the olivine data plots in the region of the Br/Cl versus I/Cl diagram occupied by MORB (Figure 3). Enrichment of I is evident in some La Palma olivines (Figure 3). Br enrichment is seen in some of the olivine samples from La Réunion and Fogo (Figure 3). Br/Cl in the Fogo olivines divides into two groups, one of which is MORB-like, while the other overlaps the range of diamond halogen concentrations (Figure 3). The highest Br/Cl analysed was in olivine and glass from Fogo. These enrichments in I and Br (relative to Cl) place some of the data obtained from La Palma, Fogo and La Réunion into compositional fields occupied by diamonds as well as serpentinites and marine pore fluids (Figure 3) (Johnson et al., 2000; Burgess et al., 2002).

Glass composition

Submarine glass shards and glassy subaerial scoria have been analysed from Pitcairn, MacDonald, Fogo, St. Helena, Tristan da Cunha, Ascension and La Palma. Glass is limited in availability and for each island between two and six individual glass analyses have been made on one to four samples (Supplementary file A). Major-, trace (Rb, Sr, Y, Zr, Nb, Ba, La, Ce) and volatile (F, Cl, S, Li, B) element compositions of the glasses were measured by EMPA (major elements primarily) and SIMS (trace and volatile concentrations primarily). These elements were selected with the aim of understanding the relationship between geochemical enrichment, volatile content and potential source variability. Selected data were originally presented in Walowski et al. (2019, 2021) but have been added to here (Supplementary file A). SiO_2 ranges from 42 to 52 wt.% and all samples plot in the basanite-basalt-trachybasalt fields (Supplementary Figure 1). There is limited evidence of differentiation within sample suites, but not between (Supplementary Figure 2). Silica saturation index (SSI) was calculated for each glass composition based on the equation given in Gill and Fitton (2022). The SSI ranges from silica-undersaturated (nepheline-normative; Fogo, MacDonald, Tristan, La Palma, St Helena, Pitcairn), to silica-saturated/oversaturated (enstatite±quartz-normative; Pitcairn, Ascension). The degree of undersaturation varies from <-20 (Fogo, MacDonald) to -15 to -10 at Tristan and La Palma and finally to >-3 at St. Helena (Figure 4). The Pitcairn samples straddle the border between undersaturation and saturation. Volcano 2 magmas have a silica-saturated composition, while Volcano 5 has SSI values similar to St. Helena glasses. The two Pitcairn islands are clearly identifiable from each other in all trace element plots with Volcano 2 distinguished by high Ba/Nb, Ti/Y, Ti/Zr and low Ce/Y (Supplementary file A). A negative relationship is observed between SSI and Nb/Zr (which decreases with increasing degree of melting) (Figure 4). Pitcairn glasses are at one end of the trend at low Nb/Zr. A similar negative relationship is also evident in Ce/Y versus SSI (not shown). There is no clear correlation between lithospheric thickness (considered to exert a control on depth of melting) and Nb/Zr in glass (Figure 4).

The TiO_2 in glass samples from St. Helena varies from 1.9 to 4.4 wt.%, clearly distinguishing them from all other OIB in this study except for those from MacDonald (4.69 wt.% TiO_2). Nb/Zr is broadly similar ~0.17±0.1, while Ba/Nb and Ce/Y are slightly lower in St Helena sample 63DS. Glasses from Ascension are silica-saturated to oversaturated (enstatite-quartz normative) and show evidence of magmatic evolution. The glasses have notably high Ti/Zr (>80) and low Ba/Nb (<4.9), Ce/Y (<1.6) and Ti/Y. Samples from Fogo are the most silica-undersaturated and have the highest Nb/Zr ratios (Figure 4). Fogo has similar trace element ratios (Ti/Zr, Ti/Y) to Tristan, but slightly lower Ba/Nb. Fogo and Tristan have similar Ce/Y ratios (average 5.8 and 6.3, respectively) which separate these samples from the other OIB (Ce/Y <3). Tristan and La Palma samples have the same SSI, but different Nb/Zr, Ce/Y, Ti/Y, Ti/Zr and Ba/Nb ratios. La Palma glasses have notably high Ti/Y and Ti/Zr similar to Ascension and St. Helena (63DS). The MacDonald seamount stands out on all trace element ratio plots with notably high Ti/Zr and Ti/Y, however, Nb/Zr is similar to La Palma.

The volatile content of the glasses is highly variable and is likely to have been affected to differing extents by degassing. Sulphur is particularly sensitive to shallow level degassing and so we use this element to indicate

ORIGINAL UNEDITED MANUSCRIPT

Downloaded from https://academic.oup.com/petrology/advance-article/doi/10.1093/petrology/egad022/7115969 by University of Edinburgh user on 18 April 2023

whether degassing has had a significant effect on the volatile concentrations. St. Helena sample 63DS has the highest S contents measured with >2000 ppm. Submarine glasses from MacDonald and Pitcairn have preserved S concentrations higher than those in MORB, ranging from 640 ppm to 1703 ppm (Supplementary file A). All the other South Atlantic OIB including Tristan, La Palma and Ascension have <210 ppm S on average and may have experienced significant loss on eruption and so volatile concentrations discussed in this section are likely to be minimum values.

Fluorine concentrations in all samples varies from ~400 ppm (Pitcairn) to >1500 ppm (Fogo) (Figure 5). Fogo glasses are remarkably enriched in F with an average concentration of 1757 ppm, compared to Pitcairn with <668 ppm. Cl and F correlate positively with Nb/Zr and Ce/Y (Figure 5).

Interaction with Cl-rich seawater would lead to higher-than-mantle Cl/K values. The Cl/K of enriched and depleted MORB is 0.01 to 0.09 (Saal et al., 2002; Arevalo and McDonough, 2010) (Figure 6). Cl/K ratios in the samples analysed here vary from 0.03 to 0.10 (Figure 6) suggesting this ratio reflects source variation rather than shallow contamination by seawater. There is no difference between samples erupted in a subaerial (Fogo, La Réunion, La Palma) versus submarine (Pitcairn, MacDonald, St. Helena) environment (Figure 6). The lowest Cl/K ratios were measured by SIMS in Fogo and Tristan alkali-rich glasses which are also enriched in Rb, Sr, Zr, Nb, La and Ce as well as F and have the lowest $\delta^{11}B$ (average -11‰) measured in glass (Walowski et al., 2021).

Additional halogen data from glass from Fogo and St. Helena were also collected using NI-NGMS. Cl/K in the glass is broadly similar to those measured by EPMA, with values ranging from 0.02 to 0.08. K/Cl does not co-vary systematically with Br/Cl. There is some variability between Br/Cl and I/Cl ratios measured in glass and in olivine, with the latter extending to higher Br/Cl than the glass from the same OIB location (Figure 3). The majority of the OIB glass data overlap those from MORB or trend towards lower I/Cl (e.g Fogo, St. Helena) (Figure 3).

Xenoliths

Additional halogen data on mantle xenoliths from La Palma were also collected using NI-NGMS. The dunite xenoliths have Cl/K in the range 0.01-0.05 (Table 3). Enrichment of I and Br is evident in some xenoliths. High I/Cl and Br/Cl may indicate that the xenoliths have been affected by seawater/marine pore fluid interaction (Figure 3).

Melt inclusions

Melt inclusion data were obtained from samples from La Réunion, Pitcairn, MacDonald (Ra), Fogo and La Palma. Details of some of major- and trace-element compositions have previously been published (Walowski et al., 2019; 2021) (Supplementary file A). New volatile data obtained by SIMS and EMPA are presented here along with SSI values (Supplementary file A). With SiO_2 ranging from 42 to 53 wt.%, the inclusions are basalt and basaltic andesite in composition (Supplementary Figure 1). SSI is similar to that of glass in the same samples, where analysed, and ranges from silica undersaturated (Fogo, MacDonald, La Palma (LP1002, 1017, 1025)) to silica-saturated (La Réunion, Pitcairn, La Palma (LP 1006)) (Figure 7). Fogo melt inclusions, as with the glass, are the most undersaturated. There is a general trend of increasing silica-undersaturation with increasing Nb/Zr, although samples from La Palma show some variability, particularly sample LP 1006 from Barranco Fagundo (Figure 7). La Réunion and Pitcairn melt inclusions cluster at low Nb/Zr (<0.15) (Figure 7), while Pitcairn has higher Ti/Y and Ba/Nb, and lower Ti/Zr than La Réunion. MacDonald inclusions again show exceptionally high Ti/Zr and Ti/Y ratios, while Fogo has the highest Nb/Zr and Ba/Nb of all analysed inclusions. Plots of Zr/Y versus La/Y suggest relative depletion in Y, indicative of garnet in the source region (Walowski et al., 2021).

ORIGINAL UNEDITED MANUSCRIPT

Downloaded from https://academic.oup.com/petrology/advance-article/doi/10.1093/petrology/egad022/7115969 by University of Edinburgh user on 18 April 2023

La Palma samples from the three different sampling localities show some clustering on trace element and halogen plots (Figure 7). Barranco Fagundo 02 sample LP1002 is silica undersaturated, has low Nb/Zr, intermediate Ba/Nb, and high Ti/Y and Ti/Zr. The remaining two samples are increasingly silica undersaturated: LP1017 (Holocene cone) has high Ba/Nb and Ti/Zr, and a similar range of F and Cl to LP1025 (1949 eruption) which has some of the highest F and Cl, similar Ba/Nb and Nb/Zr to LP1002 but lower Ti/Zr and Ti/Y.

Volatile concentrations in the melt inclusions vary between the samples but show similar patterns to the glass analyses (Figure 6). The melt inclusions extend to higher concentrations of F, Cl and S with Fogo melt inclusions most enriched (average F = 2012 ppm, Cl = 2065 ppm and S = 2619 ppm), while those from La Réunion are least enriched (average F = 370 ppm and Cl = 275 ppm), and moderate S with an average of 1570 ppm (Supplementary file A). The S analyses determined by EPMA in particular show clear evidence of subaerial degassing of glasses particularly at Ascension, Tristan and La Palma. The ratios Cl/Nb and Cl/K tend to be higher in the melt inclusions than in the glass (Figure 6), while F/Zr extends to a wider range in the melt inclusions (Figure 6). There is a general trend of increasing Nb/Zr and Ce/Y with increasing F and Cl, while SSI correlates negatively with F (Figure 7) and Cl, consistent with variable degrees of melting, with the spread of data indicating considerable source variability both within and between different OIB centres (Figure 7). We present the full dataset for both glasses and melt inclusions noting that the glass may be variably affected by degassing and so the concentrations are minimum values.

DISCUSSION

The composition of OIB reflects differences in temperature, pressure and source composition, which all influence the depth and degree of melting of discrete components in a heterogeneous mantle. Of the OIB discussed here, only La Réunion and MacDonald have been recently categorised unambiguously based on geochemical and geophysical characteristics as derived from deep-seated mantle plumes (Koppers et al., 2021). Other unambiguous deep-seated plumes have been identified beneath Afar, Easter, Galapagos, Kerguelen/Heard, Iceland, Hawai'i and Samoa. These plume-related OIB localities also display excess mantle potential temperatures, buoyancy anomalies, and high $^{3}He/^{4}He$ ratios (Courtillot et al., 2003). Pitcairn, Cape Verde and the Canary Islands are also considered to be of deep-mantle origin based on the categorization described in Koppers et al. (2021). However, the other OIB localities studied here were deemed likely (Tristan), having potential (St. Helena) and unlikely (Ascension) to be sourced from deep plumes (Koppers et al., 2021). Based on conduit connectivity in seismic tomography studies we note that Jackson et al. (2021) recently classed Tristan, St. Helena and Ascension as non-plumes. As such, we will consider that geochemical signatures at these different localities may be inherited from the deep (e.g. high $^{3}He/^{4}He$) and/or shallow mantle (e.g. low Ce/Y), and use these differences to establish where OIB potentially obtain their distinct geochemical features that often vary in space and time (e.g. Hawai'i).

Olivine composition and source discrimination

Olivine composition reflects the mantle source of the melt from which it crystallises and is impacted by temperature- and pressure-dependent mineral-melt partition coefficients (Sobolev et al., 2007; Matzen et al., 2013). Given the global distribution and range in plume influence of the sample suite, it is perhaps unsurprising that OIB in this study each have olivine with distinguishable major and trace element compositions (Figure 2a, b, c). Although olivine compositions generally overlap with published data from OIB globally (Figure 2d, e, f), key distinctions can be made.

Olivine from pyroxenite-derived melts may have higher Ni/Mg and lower Mn/Fe and Ca/Fe when compared to those that crystallise from peridotite-derived melts (Figure 2b; Sobolev et al., 2007). However, Matzen et al. (2017) have proposed that variations in Mn and Ni can equally be explained by melting fertile peridotite at

ORIGINAL UNEDITED MANUSCRIPT

Downloaded from https://academic.oup.com/petrology/advance-article/doi/10.1093/petrology/egad022/7115969 by University of Edinburgh user on 18 April 2023

variable pressure. To determine whether the observed trend in olivine compositions is related to melting of peridotite at variable pressure we regressed all olivine data to a primitive composition of Mg#=87 and plotted NiO_{87} versus MnO_{87} which shows a broadly negative trend but is not correlated with lithospheric thickness (Figure 2g). This suggests that NiO_{87} and MnO_{87} in OIB is not just affected by pressure and temperature (Matzen et al., 2017), but can reflect contributions from volatile-rich metasomatized sources. Within our dataset, olivine from Fogo and some olivine from La Palma have markedly low Ni and high Ca and Mn/Fe suggesting that carbonate-silicate melting may be important. High Ca (>2000 ppm) content in olivine from OIB can also be the result of magmas sampling a source that has been metasomatized by carbon-rich fluids (Weiss et al., 2016). The heavy halogen ratios (Br/Cl and I/Cl) determined for olivine from Fogo and La Réunion (Figure 3), are similar to those obtained from African diamonds (Burgess et al., 2002), and are consistent with a carbonated source. These results suggest that deep-mantle plumes may have variable recycled and metasomatized components in their sources. However, olivine composition, although informative, cannot unambiguously discriminate between different source contributions, but indicates that the OIB samples analysed here are not derived solely from dry peridotite melting.

The lithospheric lid

Lithospheric thickness plays an important role in the generation of melt in the upper mantle (e.g. Niu and O'Hara, 2008; Niu & Green, 2018). For example, mantle melting beneath mid ocean ridges begins at pressures around 2 GPa and extends to ~22% melting beneath the ridge axis (Niu, 1997). Melt generation is thought to primarily occur in the upper mantle where the dominant rock type is peridotite, but is influenced by contributions from pyroxenite and eclogite (e.g. Prytulak and Elliott, 2007), recycled components (e.g., fresh and altered oceanic lithosphere, continental lithosphere, and sediments; White, 2015) and carbonated mantle (Hanyu et al., 2019). Excess temperature and/or the presence of volatiles from recycled components can extend the onset of melting to greater pressures than observed at ocean ridges. Small-degree melts (1-5%) are particularly enriched in incompatible elements including volatiles. Previous modelling of the OIB of interest here has demonstrated that the trace element ratios from across the sample suite are consistent with variations in the degree of partial melting at depth, predominantly in the garnet facies peridotite mantle (2–10% melt) followed by near-surface fractionation of some samples (Walowski et al., 2021). These smaller-degree melts tend to be more alkali rich and are silica undersaturated. The majority of OIB glasses are alkali rather than sub-alkali (tholeiitic), although tholeiitic compositions may also occur (e.g., Hawai'i and La Réunion) where mantle temperature anomalies are recorded (Garcia et al., 2016; Walowski et al., 2019). Small-fraction melting tends to occur at higher pressures, and a correlation between increasing oceanic lithospheric thickness and small-fraction, high-pressure melting has been proposed (Humphreys and Niu, 2009). It is therefore important to be aware of differences in lithospheric thickness when comparing OIB from different islands.

Here, we compare lithospheric thickness and incompatible trace element ratios indicative of melting extent (e.g., Nb/Zr) to again assess the role of lithospheric thickness (Figure 4). Lithospheric thickness variations extracted from LITHO0.1 (Pasyanos et al., 2014) at the ocean islands discussed here ranges from ~40 to ~70 km (Figure 4). Only Fogo, Hawai'i and La Réunion have lithospheric lids >60 km thick, with Fogo erupting through the thickest lithosphere. All these OIB (Fogo, Hawai'i and La Réunion) have inferred mantle buoyancy fluxes in excess of 10^3 kg s^{-1} and high $^3He/^4He$ ratios (Courtillot et al., 2003). However, magmas erupted in Hawai'i and La Réunion include both alkali and sub-alkali compositions indicative either of more extensive melting in the upper mantle than is evident at Fogo, or the presence of pyroxenite in the mantle source (Figure 4).

Tristan and Ascension magmas have erupted through lithosphere that is <45km thick, consistent with their position close to the mid-Atlantic ridge. The remaining ocean islands (Pitcairn, MacDonald, La Palma, St. Helena and Iceland (off-axis)) erupt through lithosphere of between 50 and 55 km thick. Figure 4 shows a comparison of these estimated lithospheric thicknesses and Nb/Zr (glass and melt inclusions); a lack of correlation between

ORIGINAL UNEDITED MANUSCRIPT

Downloaded from https://academic.oup.com/petrology/advance-article/doi/10.1093/petrology/egad022/7115969 by University of Edinburgh user on 18 April 2023

these two parameters suggests that the lithospheric lid alone is unable to explain trace element variability between OIB globally. This is consistent with the regression modelling of the olivine compositional dataset that shows no correlation between NiO_{87}, MnO_{87} and lithosphere thickness (Figure 2g) and suggests an important role for volatiles.

Partial melting and silica saturation

Although some of the differences among OIB may be attributed to the lithospheric lid effect, it is clear that potential temperature, source composition and assimilation of different contaminants (recycled continental and ocean crust, sediments, lithospheric mantle and carbonate and their low-temperature, low-pressure alteration products) are important in determining OIB composition. For example, unlike La Réunion or Pitcairn, Fogo is considered to sample a mixed source with contributions from a moderate HIMU endmember (altered oceanic crust) and an EM1-like endmember (continental crust and continental lithospheric fragments) based on Sr-Nd-Pb isotope ratios and light $\delta^{11}B$ isotope signatures (Escrig, et al., 2005; Walowski et al., 2021). The Cape Verde islands host oceanic carbonatites, suggesting local enrichment in a carbonate component (Jørgensen & Holm, 2002). Increasing the abundances of volatiles (e.g., H_2O and CO_2) and alkalis will lower the solidus temperature and raise the depth of onset of melting (Wyllie, 1988). For example, melting can be initiated at pressures up to 12 GPa with source lithologies that have 100-1000 ppm CO_2 (Dasgupta et al., 2009). Furthermore, for a given P–T path, the integrated degree of melting undergone by a homogeneous peridotitic mantle is lower than the degree of melting of the same peridotite veined by pyroxenites, suggesting that source composition variability (in addition to volatiles) has a direct effect on the degree of melting and volume of melt extracted (Brunelli et al., 2018). Both F and Cl also depress the liquidus temperature in basaltic systems (and therefore the mantle solidus) and complex with Mg and Fe respectively, thus affecting mineral-melt partitioning (Filiberto et al., 2012).

Simple decompression melting calculations on mantle peridotite were made using the model of Fitton et al. (2021) in which the mantle adiabatic gradient is 0.3°C/km until it crosses the dry solidus whereupon melt is produced at a rate of 0.4%/km (Figure 7). Incompatible-element concentrations in accumulated non-modal batch melts at each stage were calculated from the weighted average composition of each 1 km (0.4% melt) decompression step (see Fitton et al., 2021 for details of source composition, melting modes and D-values used). The silica saturation index (SSI) was calculated from the average melt fraction and pressure at each decompression stage, based on melt compositions reported by Hirose and Kushiro (1993) in their experiments on fertile peridotite HK-66. Least-squares regression of SSI, melt fraction (F, expressed as mass %) and pressure (P in GPa) fit these data closely (RMSD of SSI=2.25; Gill and Fitton, 2022) to a plane with the equation:

$$SSI = 0.6707F - 4.957P – 8.963.$$

The model was run with potential temperatures of 1300, 1400 and 1500°C (Figure 7), and to achieve the high Nb/Zr (>0.15) and Ce/Y ratios (up to 6.4) evident in the OIB samples analysed here, melting has to start in the garnet stability field and at potential temperatures >1400°C, if the mantle source is dry peridotite. However, the failure of the model to fit the Nb/Zr and SSI data implies that simple decompression melting of dry peridotite cannot account for the compositional range of OIB (Figure 7). Addition of volatiles would allow melting to occur at greater depths and over a wider temperature range, but in all cases the calculated degree of melting is <6%, with the highest Nb/Zr and Ce/Y values from Fogo and Tristan produced by <1% melting (Figure 7), which is remarkably low. This suggests that other components such as carbonated peridotite or eclogite (e.g. Kiseeva et al., 2013), carbonate-rich silicate melt (as proposed to explain the wide range in Hawai'i SSI; Dixon et al., 2008; Sisson et al., 2009) or supercritical fluids (Ni et al., 2017) are potentially involved in the genesis of these OIB.

ORIGINAL UNEDITED MANUSCRIPT

Downloaded from https://academic.oup.com/petrology/advance-article/doi/10.1093/petrology/egad022/7115969 by University of Edinburgh user on 18 April 2023

Role of volatiles including halogens

The presence of carbonate throughout the mantle has a potentially profound impact on the composition of OIB, and the importance of carbonate during melting at variable depths from 410 km to the core-mantle boundary is increasingly being recognised (e.g. Kiseeva et al., 2013; Mazza et al., 2016; Hanyu et al., 2019). Carbon dioxide is an abundant volatile species in OIB magmas, and is thought to be derived from a range of sources, including carbonate-silicate melts, carbonated metasomatised peridotite, carbonated AOC or marine carbonate (e.g. Ionov, 1998). Carbonate (*sensu lato*) may therefore be distributed throughout different reservoirs in the mantle. However, measuring primary or source concentrations of CO_2 in erupted magmas is challenging due to its volatile nature. Recent work has demonstrated that even melt inclusion compositions, which have been used as a primary method for determining CO_2, can be modified significantly through post-entrapment CO_2 diffusion into vapour bubbles (upwards of 40-90% loss; Rasmussen et al., 2020 and references therein). Here, we lack sufficient information to accurately correct for post-entrapment CO_2 -loss, and therefore we do not discuss the concentrations of CO_2 directly. Rather, we have measured halogen contents in both glass and melt inclusions in the OIB samples used in this study. In most, but not all, cases the glass halogen values are within the range measured in the corresponding melt inclusions, which extend to higher values (Figure 5; Supplementary file A). The halogen contents of the glass from OIB samples are therefore considered minimum values. The halogen concentrations measured by SIMS in both glass and melt inclusions suggest that the majority of OIB magmas are volatile-rich, containing between 309 and 2637 ppm F, up to 2600 ppm Cl (Figure 5) and up to 3500 ppm S.

The calculated SSI combined with halogen and incompatible element ratios are used to explore the nature of the carbonate component using key comparisons from Hawai'i and Cook-Austral (Dixon et al., 2008; Sisson et al., 2009; Hanyu et al., 2019). Halogen concentrations and ratios to incompatible lithophile elements such in K, P, Nb, Zr and Ti can potentially fingerprint different source contributions (e.g. Hanyu et al., 2019), especially if combined with SSI. For example, melting of a pyroxenite source would increase silica saturation, and potentially F concentrations. We rule out addition of halogens via supercritical fluids because investigations of volcanic spherules condensed from supercritical fluids are Si-, Ca- and Na-rich but Al-poor (Kirstein et al., 2021) and their addition would increase SSI.

Carbonated phlogopite source?

The diverse range of potential carbonate and other recycled contaminants in mantle source regions is important. Not all carbonate will have the same effect on OIB composition. Enrichment of OIB source regions by carbonate-rich melts (e.g. carbonatites) or carbon-rich fluids would result in considerable trace element source variability including increased Sr, P and halogen concentrations. For example, the composition of the early high-S Kilauea basanite-nephelinite suite is proposed to originate from a carbonated phlogopite-garnet peridotite source with moderately high CO_2 concentrations (Sisson et al., 2009). The SSI calculated for these early Kilauea magmas is much lower (-36 to -50) than typical peridotite melts (Figure 4) and corresponds with elevated Rb, Sr, Ba, Nb and Cl concentrations from melting of a fertile domain in the ambient upper mantle (Sisson et al., 2009) (Figure 4 (red triangles)). Early, high-S Kilauea samples are clearly distinguishable and very different from all OIB discussed here (Figure 4, 6), suggesting that such a source is not commonly tapped and/or preserved in the composition of OIB. Finally, phlogopite-bearing mantle sources produce melts with distinct Cl/K ratios. In the high-S glasses sampled from these early Kilauea magmas, Cl/Nb is in the range 40-50, much higher than all other OIB analysed here, while Cl/K is <0.1 (Figure 6), again supporting a source at Kilauea that is uncommon and distinctive from OIB globally.

Dominantly peridotite mantle source

ORIGINAL UNEDITED MANUSCRIPT

Downloaded from https://academic.oup.com/petrology/advance-article/doi/10.1093/petrology/egad022/7115969 by University of Edinburgh user on 18 April 2023

In the new OIB dataset presented here, we find SSI, halogen, and trace element variability in La Réunion and Pitcairn samples that are distinct (Figure 6, 7, and 8). Pitcairn and La Réunion magmas form beneath lithosphere of variable thickness (Pitcairn ~ 50km; La Réunion ~60 km). Both La Réunion and Pitcairn trend towards silica-saturation, have low (<1000 ppm) halogen concentrations, low F/Zr and Nb/Zr, a reflection of their sub-alkali composition and production by greater degrees of melting at shallow depths (Walowski et al., 2019; 2021). They can be distinguished from each other through their Ba/Nb and Ti/Zr ratios, consistent with the Pitcairn EM1 geochemical signal (Woodhead & Devey, 1993). Pitcairn also trends towards marginally higher F and Cl, although average values between Volcano 2 and Volcano 5 differ substantially (Volcano 2: average F =381 ppm; average Cl =298 ppm; Volcano 5: average F =518 ppm; average Cl =520 ppm). Volcano 2 magmas were slightly more evolved (SiO_2 >50 wt%, lower FeO) suggesting shallow fractionation and loss of volatiles. The lithospheric thickness is the same for both Pitcairn volcanoes, so small-scale local source variability may also be important.

Halogen and incompatible element values at La Réunion are closer to those of Pitcairn Volcano 2, consistent with a small amount of recycled material being present in the La Réunion plume (Valer et al., 2017), probably as distributed fertile veins. The low CaO/Al_2O_3 ratios and high SiO_2 in Pitcairn lavas may indicate a pyroxenitic source component in those lavas, which would drive SSI to positive values and may explain some of the scatter in the melt inclusion data. As both La Réunion and Pitcairn originate from deep-seated plumes there is ample opportunity to incorporate components *en route* to the surface (Figure 9). In sum, the La Réunion and Pitcairn magmas appear to have formed by peridotite melting and assimilation of other components (e.g. pyroxenite or carbonate).

Eclogite-derived carbonate and Ti variability

Eclogite (formed from deeply subducted mafic ocean crust), due to its lower solidus temperature when compared to peridotite, may contribute disproportionately to melting despite its limited distribution in the mantle (Kiseeva et al., 2012). Eclogites are a potential reservoir of volatiles and incompatible trace elements in the mantle, especially in the mantle transition zone (Figure 9). Eclogite melting experiments have produced co-existing carbonate and silicate melts at low to intermediate degrees of melting over a range of pressures from 3.5 to 5.5 GPa (Kiseeva et al., 2012). Experimental studies in which carbonated eclogite and lherzolite are melted at progressively higher temperatures and at asthenospheric pressures (3 GPa) produce carbonatite melt followed by strongly silica-undersaturated silicate melt which can co-exist at a range of temperatures (Dasgupta et al., 2005, 2006, 2007). Partial melting of carbonate-bearing mantle rocks produces melts with high CaO and low SiO_2 contents (Dasgupta et al., 2006). Melting of a heterogeneous carbonated mantle could also result in metasomatism of the surrounding peridotite, which could subsequently be partially melted to produce melts with high concentrations of incompatible trace elements and volatiles (Dasgupta et al., 2006; Dixon et al., 2008). Repeated melting of these heterogeneities would provide ample opportunity to introduce geochemical variability in OIB.

The Niihau (Hawai'i) volcanic rocks are proposed to originate from melting peridotite that has been metasomatised by carbonatite (Dixon et al., 2008). The melts are mildly undersaturated (SSI -4 to -7) and plot at higher Nb/Zr and lower TiO_2 and Cl than other Hawai'i compositions (Figure 4, 8). Melting of carbonated peridotite produces melts that have lower TiO_2 and FeO* (total Fe expressed as FeO) than most OIB (Dasgupta et al., 2007). The Niihau Kiekie basalts have remarkably low Rb, Sr, Nb, Zr and Cl concentrations, low TiO_2, moderate S and Nb/Zr ratios (Dixon et al., 2008; Figure 4, 8). Plotting F concentration against SSI and Ce/Y shows clear linear relationships, with F and Ce/Y increasing with decreasing SSI (e.g Figure 7). This suggests that the low SSI values of <-20 are correlated with increased volatile contents in the source and potentially explains why Fogo, which has the greatest lithospheric thickness (~70 km), can produce small-degree melt (elevated Nb/Zr of >0.3) at depth (Figure 7). Tristan has similar Ce/Y ratios to Fogo, erupts through lithosphere that is

ORIGINAL UNEDITED MANUSCRIPT

Downloaded from https://academic.oup.com/petrology/advance-article/doi/10.1093/petrology/egad022/7115969 by University of Edinburgh user on 18 April 2023

much thinner (~43 km) and appears to have a mantle source that is not as enriched in halogens (although only glass data are available for Tristan and so are potentially minimum values at 1075 ppm F and >900 ppm Cl). This suggests that the volatile content rather than lithospheric thickness may be the dominant control on melt generation in some OIB, and that variations in the OIB-source mantle may be caused by mixing of pyroxenitic, carbonate-enriched, and peridotitic (depleted upper mantle) components.

Melting of other lithologies must be important because TiO_2 varies between 2.1 and 4.5 wt. % (Figure 8). A significant contribution from carbonate-free eclogite melting would lead to silica-oversaturated melts, while the majority of OIB are silica-undersaturated. Carbonated eclogite can be subducted to between 300 and 600 km depth and when melted can produce silicate and carbonate melts (Kiseeva et al., 2012; Elazar et al., 2019). Carbonated lherzolite melting experiments suggest that the melt produced is silica-undersaturated and enriched in Ti (Dasgupta et al., 2006). It has been proposed that melting veins of carbonated garnet pyroxenite (containing 5 wt.% CO_2) in a host peridotite could produce a carbonatitic liquid and an immiscible, Ti-enriched silica-undersaturated silicate liquid because the pyroxenite could be melted without fusion of the surrounding peridotite (Dasgupta et al., 2006; Prytulak & Elliott, 2007).

Titanium and F are both considered moderately incompatible elements in the upper mantle. The TiO_2 contents of the melt inclusions vary and positively correlate with F, with distinct trends emerging (Figure 8). The La Réunion, Pitcairn and Macdonald trend passes through MORB and extends to higher TiO_2 and volatile concentrations (Figure 8). This is consistent with mixing of depleted and enriched source components in these deep-mantle plumes. Overall, the data form a fan-shaped array with the upper boundary of halogen data defined by Fogo (SiO_2: 42-46 wt.%; MgO 4.7 – 6 wt.%) with high TiO_2 and high F and Cl (Figure 8). La Palma, Tristan and early Kilauea alkali basalts (SiO_2: 42-48 wt.%; MgO: 5 – 10 wt.%) lie between the two trends (Figure 8). Tholeiitic glass (46-48 wt. % SiO_2; 5-6 wt. % MgO) from Kilauea (Sisson et al., 2009) plots at lower F possibly due to volatile loss (Figure 8).

Enrichment of Ti can result from a variety of different sources but only MORB, altered oceanic crust and silica-undersaturated melts from carbonated eclogite have initial TiO_2 >1 wt.% (Dasgupta et al., 2006; Prytulak & Elliott, 2007). It has been estimated that percent-level addition of a recycled mafic oceanic crust component to peridotitic melts can give rise to substantial variations in TiO_2 (Prytulak & Elliott, 2007). Melting of carbonated, anhydrous pyroxenite could also produce a Ti-enriched silica-undersaturated melt as well as a carbonatitic liquid (Kiseeva et al., 2012). Mixing of these components would result in Ti enrichment but should also have a distinguishable halogen signature.

Assuming limited contamination in the near-surface environment as suggested from boron isotopes (Walowski et al., 2021), F and Cl in primitive magmas should reflect the halogen contents of the mantle source or may reflect mixing of melts from different source components. F (and Cl) do not show the same behaviour as S, with some of the lowest halogen concentrations preserved in La Réunion melt inclusions, which have S contents ranging from 1352 to 1789 ppm. Hanyu et al. (2019) suggested that Cl, when ratioed with lithophile elements (K, Nb), could be used to identify melts from altered and carbonated oceanic crust. Ratios including F/P, F/Zr, F/Ti, Cl/K, Cl/P and Cl/Nb should be minimally fractionated during mantle melting and subsequent fractional crystallisation, and should reflect source variability. Plots of Cl/Nb versus Cl/K indicate that OIB show a range in halogen/lithophile-element ratios extending from depleted mantle MORB-like values to highly enriched (Figure 7). All OIB classed as HIMU analysed here (La Palma, St. Helena) as well as those with a HIMU component (e.g. MacDonald) fall on an extension of the mixing trend identified for the Cook-Austral islands between MORB-mantle melt and carbonated, altered ocean crust (Figure 6) (Cabral et al., 2014; Hanyu et al., 2019). Not all these islands are thought to be the product of deep-mantle plumes (Koppers et al., 2021), which suggests that the HIMU signature may be pervasive in the MTZ or upper mantle.

ORIGINAL UNEDITED MANUSCRIPT

Downloaded from https://academic.oup.com/petrology/advance-article/doi/10.1093/petrology/egad022/7115969 by University of Edinburgh user on 18 April 2023

Altered oceanic crust (AOC) has Cl/Nb of ~60 and Cl/K >0.2 (Hanyu et al., 2019). If AOC is the main reservoir contributing Cl to the mantle, it follows that the range in Cl/Nb may be linked to the extent of dehydration that the AOC undergoes during subduction ultimately leading to lower Cl/Nb and/or variable mixing of depleted mantle and AOC (Figure 6). The fourfold difference in Cl/K between Pitcairn and La Palma melt inclusions could result from preferential loss of K during slab subduction (high Cl/K) or a difference in assimilant, e.g. carbonated eclogite or metasomatised peridotite (lower Cl/K). As HIMU OIB extend to higher Cl/K, the variability between different HIMU domains could be linked to the age, or extent of alteration, of the subducting slab with increasing loss of K as the subducted slab is disaggregated. Note La Palma is classed as a young HIMU island and extends to higher Cl/K than St. Helena, which has a more pronounced (older?) HIMU component.

Carbonate in the HIMU reservoir

Carbonated altered oceanic crust has impacted the geochemical composition of the OIB that have HIMU source signatures including La Palma, St. Helena and MacDonald (Figure 6, 8). Mixing of a depleted N-MORB-like component with a metasomatised peridotite component could explain some of the compositional variability (e.g. high Ce/Y, low Cl/Nb). Fogo OIB, which may represent mixing between HIMU and EM1 source endmembers (Escrig et al., 2005; Walowski et al., 2021) appears to have an intermediate composition in Cl/Nb-Cl/K space between the HIMU and enriched trends (Figure 6). This observation is consistent with previous interpretations suggesting that both subduction-modified AOC and an additional carbonate-modified source component may be important. Br/I in some of the Fogo olivines overlap diamond halogen analyses, suggesting deep entrainment. As part of the Cape Verde archipelago with one of the few oceanic carbonatite occurrences, the mantle source is known to be carbonate rich (Jørgensen & Holm, 2002). However, the distinctive geochemical signature at Fogo is not the same as at Niihau where carbonatite metasomatism of the source has been invoked (Figure 8).

OIB from Fogo has the highest F and Cl concentrations measured (as well as high Ba and Nb/La), the lowest SSI and remarkable incompatible trace element enrichment (Figure 8). F/Zr ratios highlight the particularly F-rich nature of the Fogo basalts (Figure 8). This suggests that both the nature of the carbonate enrichment and the extent of metasomatism of the source is important in melt generation at Fogo. We suggest that upward-migrating interstitial carbonate–silicate liquids have a profound influence on melting especially beneath thick lithosphere, in part because such liquids are enriched in volatiles that lower the solidus and promote melting of fusible material at greater depth. The source of these melts may be carbonated eclogite in order to generate the degree of silica undersaturation and Ti enrichment (e.g. Figure 8). Fogo sits on the thickest lithosphere of all the islands considered in this study (>68 km) and has the most enriched source of all OIB investigated.

Pervasive heterogeneity in the mantle

Recent models for the origin of HIMU mantle components suggest that HIMU OIB result from the mixing of melts from subducted altered oceanic lithosphere with MORB-like peridotite melts and a carbonate component. The mantle transition zone is an underestimated reservoir of volatile and incompatible trace element enrichment (e.g. Pearson et al., 2014) as slabs can stall there and may be an important contributor to mantle heterogeneity, particularly the formation of a shallow HIMU component. Plumes, including the one inferred at Pitcairn, may initiate deep but then interact with recycled components *en route* to the surface.

Entrainment of material within mantle plumes can vary both temporally and spatially. Such a process is consistent with the volatile content of different OIB samples and the diversity seen in ocean island chains that is unrelated to upper mantle melting processes. The dominantly peridotitic mantle may have carbonated components along with recycled altered oceanic crust (e.g. Dasgupta et al., 2010) stirred into it via convection (Figure 9). Decompression of this highly heterogeneous, fusible source material would facilitate (re)melting and

ORIGINAL UNEDITED MANUSCRIPT

Downloaded from https://academic.oup.com/petrology/advance-article/doi/10.1093/petrology/egad022/7115969 by University of Edinburgh user on 18 April 2023

provide ample potential heterogeneity in the composition of OIB. The peridotite assemblage produces smaller melt fractions than either pyroxenite or eclogite at the same temperature and pressure due to their respective mineral assemblages, particularly the proportions of olivine, pyroxene and garnet. The SSI and melt inclusion compositional data determined for OIB in this study suggest that the contribution of pyroxenite is limited. Fogo OIB, which is the most enriched in F and incompatible elements is also the most silica-undersaturated. Volatile-triggered melting of carbonated metasomatized peridotite or eclogite appears key to melting at Fogo and other OIB where SSI is low, and F, Cl, TiO_2 and CaO are high.

Conclusions

(i) Ocean island basalts record heterogeneity at a variety of scales as seen when comparing tholeiitic and alkali basalt compositions. Increased degrees of melting (and assimilation), as evident at La Réunion and Pitcairn, mask some of the initial source signatures. Simple, variable peridotite melting is not sufficient to explain the compositional variation of OIB.

(ii) Volatiles facilitate melting at greater depths and beneath thick lithosphere, e.g. where the CO_2-saturated solidus is intersected, and the resultant melt is highly enriched in both incompatible elements and in volatiles as proposed here for Fogo.

(iii) Fluorine co-varies strongly with the highly incompatible Cl and with TiO_2, suggesting that Ti-rich silica-undersaturated melts which require a contribution from carbonated, metasomatized peridotite or eclogite may be ubiquitous in the source of OIB, together with an AOC component.

Acknowledgements

For analytical assistance we thank J. Craven (SIMS), R. Hinton (SIMS), S. Kearns (EPMA) and C. Hayward (EPMA). We thank C. Devey for access to samples in the GEOMAR collection. Funding was provided by National Environmental Research Council grant NE/M000443/1 and EIMF proposals IMF573/1015 and IMF590/0516. The editor, Adam Kent, and two anonymous reviewers are thanked for their insightful comments.

Data availability

New data underlying this article are available in the article and in its online supplementary material. Published data by the authors used extensively in the article are available from GEOROC http://georoc.mpch-mainz.gwdg.de/georoc/ GEOROC-Citation-ID: 24778.

ORIGINAL UNEDITED MANUSCRIPT

Downloaded from https://academic.oup.com/petrology/advance-article/doi/10.1093/petrology/egad022/7115969 by University of Edinburgh user on 18 April 2023

731 Ackermand, D., Hekinian, R., & Stoffers, P. (1998). Magmatic sulfides and oxides in volcanic rocks from the
732 Pitcairn hotspot (South Pacific). *Journal of Mineralogy & Petrology, 64*(1-4), 149-162.

733 Bonifacie, M., Busigny, V., Mével, C., Philippot, P., Agrinier, P., Jendrzejewski, N., et al. (2008). Chlorine isotopic
734 composition in seafloor serpentinites and high-pressure metaperidotites. Insights into oceanic serpentinization
735 and subduction processes. *Geochimica et Cosmochimica Acta, 72*(1), 126-139.
736 https://www.sciencedirect.com/science/article/pii/S0016703707005819

737 Broadley, M. W., Ballentine, C. J., Chavrit, D., Dallai, L., & Burgess, R. (2016). Sedimentary halogens and noble
738 gases within Western Antarctic xenoliths: Implications of extensive volatile recycling to the sub continental
739 lithospheric mantle. *Geochimica et Cosmochimica Acta, 176*, 139-156.
740 https://www.sciencedirect.com/science/article/pii/S0016703715007073

741 Broadley, M. W., Barry, P. H., Ballentine, C. J., Taylor, L. A., & Burgess, R. (2018). End-Permian extinction
742 amplified by plume-induced release of recycled lithospheric volatiles. *Nature Geoscience, 11*(9), 682-687.
743 https://doi.org/10.1038/s41561-018-0215-4

744 Broadley, M. W., Sumino, H., Graham, D. W., Burgess, R., & Ballentine, C. J. (2019). Recycled Components in
745 Mantle Plumes Deduced From Variations in Halogens (Cl, Br, and I), Trace Elements, and 3He/4He Along the
746 Hawaiian-Emperor Seamount Chain. *Geochemistry, Geophysics, Geosystems, 20*(1), 277-294.
747 https://doi.org/10.1029/2018GC007959. https://doi.org/10.1029/2018GC007959

748 Brazzle R. H., Pravdivtseva 0. V., Meshik A. P., & Hohenberg C.M. (1999). Verification and interpretation of I-Xe
749 chronometer. *Geochimica et Cosmochimica Acta*, 63, 739-769.

750 Brunelli, D., Cipriani, A., & Bonatti, E. (2018). Thermal effects of pyroxenites on mantle melting below mid-
751 ocean ridges. *Nature Geoscience, 11*(7), 520-525. https://doi.org/10.1038/s41561-018-0139-z

752 Burgess, R., Layzelle, E., Turner, G., & Harris, J. W. (2002). Constraints on the age and halogen composition of
753 mantle fluids in Siberian coated diamonds. *Earth and Planetary Science Letters*, 197(3), 193-203.
754 https://www.sciencedirect.com/science/article/pii/S0012821X02004806

755 Cabral, R. A., Jackson, M. G., Koga, K. T., Rose-Koga, E. F., Hauri, E. H., Whitehouse, M. J., et al. (2014). Volatile
756 cycling of H2O, CO2, F, and Cl in the HIMU mantle: A new window provided by melt inclusions from oceanic hot
757 spot lavas at Mangaia, Cook Islands. *Geochemistry, Geophysics, Geosystems, 15*(11), 4445-4467.
758 https://doi.org/10.1002/2014GC005473. https://doi.org/10.1002/2014GC005473

759 Chaussidon, M., & Marty, B. (1995). Primitive Boron Isotope Composition of the Mantle. *Science*, 269(5222),
760 383.

761 Chavrit, D., Burgess, R., Sumino, H., Teagle, D. A. H., Droop, G., Shimizu, A., & Ballentine, C. J. (2016). The
762 contribution of hydrothermally altered ocean crust to the mantle halogen and noble gas cycles. *Geochimica et*
763 *Cosmochimica Acta, 183*, 106-124. https://www.sciencedirect.com/science/article/pii/S0016703716301156

764 Christensen, U. R., & Hofmann, A. W. (1994). Segregation of subducted oceanic crust in the convecting mantle.
765 *Journal of Geophysical Research: Solid Earth, 99*(B10), 19867-19884. https://doi.org/10.1029/93JB03403.
766 https://doi.org/10.1029/93JB03403

767 Clarke, E., De Hoog, J. C. M., Kirstein, L. A., Harvey, J., & Debret, B. (2020). Metamorphic olivine records
768 external fluid infiltration during serpentinite dehydration. *Geochemical Perspectives Letters, 16*, 25-29.
769 http://www.geochemicalperspectivesletters.org/article2039

ORIGINAL UNEDITED MANUSCRIPT

Downloaded from https://academic.oup.com/petrology/advance-article/doi/10.1093/petrology/egad022/7115969 by University of Edinburgh user on 18 April 2023

Courtier, A. M., Bagley, B., & Revenaugh, J. (2007). Whole mantle discontinuity structure beneath Hawaii. *Geophysical Research Letters, 34*(17). https://doi.org/10.1029/2007GL031006. https://doi.org/10.1029/2007GL031006

Courtillot, V., Davaille, A., Besse, J., Stock, J. (2003). Three distinct types of hotspots in the Earth's mantle. *Earth and Planetary Science Letters, 205*, 295-308.

Danyushevsky, L. V., & Plechov, P. (2011). Petrolog3: Integrated software for modeling crystallization processes. *Geochemistry, Geophysics, Geosystems, 12*(7). https://doi.org/10.1029/2011GC003516. https://doi.org/10.1029/2011GC003516

Dasgupta, R., Hirschmann, M. M., McDonough, W. F., Spiegelman, M., & Withers, A. C. (2009). Trace element partitioning between garnet lherzolite and carbonatite at 6.6 and 8.6 GPa with applications to the geochemistry of the mantle and of mantle-derived melts. *Chemical Geology, 262*(1), 57-77. https://www.sciencedirect.com/science/article/pii/S0009254109000667

Dasgupta, R., Hirschmann, M. M., & Dellas, N. (2005). The effect of bulk composition on the solidus of carbonated eclogite from partial melting experiments at 3 GPa. *Contributions to Mineralogy and Petrology, 149*(3), 288-305. https://doi.org/10.1007/s00410-004-0649-0

Dasgupta, R., Hirschmann, M. M., & Stalker, K. (2006). Immiscible Transition from Carbonate-rich to Silicate-rich Melts in the 3 GPa Melting Interval of Eclogite + CO2 and Genesis of Silica-undersaturated Ocean Island Lavas. *Journal of Petrology, 47*(4), 647-671. https://doi.org/10.1093/petrology/egi088

Dasgupta, R., Hirschmann, M. M., & Smith, N. D. (2007). Partial Melting Experiments of Peridotite + CO2 at 3 GPa and Genesis of Alkalic Ocean Island Basalts. *Journal of Petrology, 48*(11), 2093-2124. https://doi.org/10.1093/petrology/egm053

Debret, B., Koga, K. T., Cattani, F., Nicollet, C., Van den Bleeken, G., & Schwartz, S. (2016). Volatile (Li, B, F and Cl) mobility during amphibole breakdown in subduction zones. *Lithos*, 244, 165-181. https://www.sciencedirect.com/science/article/pii/S0024493715004466

Devey, C., Ackermand, D., Binard, N., Chmarzynski, P., Franke-Bruckmaier, B., Geldmacher, J., & Hemond, B. (1993). *Cruise Report SO-84: The St Helena Hotspot. Las Palmas-Cape Town 02.01. 93-20.02. 93.*: Geologische-Palaontologisches Institut und Museum, Christian-Albrechts-Universitat, Kiel.

Dixon, J., Clague, D. A., Cousens, B., Monsalve, M. L., & Uhl, J. (2008). Carbonatite and silicate melt metasomatism of the mantle surrounding the Hawaiian plume: Evidence from volatiles, trace elements, and radiogenic isotopes in rejuvenated-stage lavas from Niihau, Hawaii. *Geochemistry, Geophysics, Geosystems, 9*(9). https://doi.org/10.1029/2008GC002076. https://doi.org/10.1029/2008GC002076

Dixon, J. E., Bindeman, I. N., Kingsley, R. H., Simons, K. K., Le Roux, P. J., Hajewski, T. R., et al. (2017). Light Stable Isotopic Compositions of Enriched Mantle Sources: Resolving the Dehydration Paradox. *Geochemistry, Geophysics, Geosystems*, 18(11), 3801-3839. https://doi.org/10.1002/2016GC006743. https://doi.org/10.1002/2016GC006743

Dobson, D. P., & Brodholt, J. P. (2005). Subducted banded iron formations as a source of ultralow-velocity zones at the core–mantle boundary. *Nature, 434*(7031), 371-374. https://doi.org/10.1038/nature03430

Elazar, O., Frost, D., Navon, O., & Kessel, R. (2019). Melting of H2O and CO2-bearing eclogite at 4–6 GPa and 900–1200 °C: Implications for the generation of diamond-forming fluids. *Geochimica et Cosmochimica Acta*, 255, 69-87. https://www.sciencedirect.com/science/article/pii/S0016703719301838

ORIGINAL UNEDITED MANUSCRIPT

Downloaded from https://academic.oup.com/petrology/advance-article/doi/10.1093/petrology/egad022/7115969 by University of Edinburgh user on 18 April 2023

Escrig, S., Doucelance, R., Moreira, M., & Allègre, C. J. (2005). Os isotope systematics in Fogo Island: Evidence for lower continental crust fragments under the Cape Verde Southern Islands. *Chemical Geology, 219*(1), 93-113. https://www.sciencedirect.com/science/article/pii/S000925410500094X

Feng, X., Steiner, Z., & Redfern, S. A. T. (2021). Fluorine incorporation into calcite, aragonite and vaterite CaCO3: Computational chemistry insights and geochemistry implications. *Geochimica et Cosmochimica Acta*, 308, 384-392. https://www.sciencedirect.com/science/article/pii/S0016703721003021

Filiberto, J., Wood, J., Dasgupta, R., Shimizu, N., Le, L., & Treiman, A. H. (2012). Effect of fluorine on near-liquidus phase equilibria of an Fe–Mg rich basalt. *Chemical Geology*, 312-313, 118-126. https://www.sciencedirect.com/science/article/pii/S0009254112001817

Fischer, K. M., Ford, H. A., Abt, D. L., & Rychert, C. A. (2010). The Lithosphere-Asthenosphere Boundary. *Annual Review of Earth and Planetary Sciences, 38*(1), 551-575. https://doi.org/10.1146/annurev-earth-040809-152438

Fitton, J. G., Williams, R., Barry, T. L., & Saunders, A. D. (2021). The Role of Lithosphere Thickness in the Formation of Ocean Islands and Seamounts: Contrasts between the Louisville and Emperor–Hawaiian Hotspot Trails. *Journal of Petrology, 61*(11-12). https://doi.org/10.1093/petrology/egaa111

French, S. W., & Romanowicz, B. (2015). Broad plumes rooted at the base of the Earth's mantle beneath major hotspots. *Nature, 525*(7567), 95-99. https://doi.org/10.1038/nature14876

Garcia, M. O., Weis, D., Jicha, B. R., Ito, G., & Hanano, D. (2016). Petrology and geochronology of lavas from Ka'ula Volcano: Implications for rejuvenated volcanism of the Hawaiian mantle plume. *Geochimica et Cosmochimica Acta, 185*, 278-301. https://www.sciencedirect.com/science/article/pii/S001670371630134X

Gazel, E., Trela, J., Bizimis, M., Sobolev, A., Batanova, V., Class, C., & Jicha, B. (2018). Long-Lived Source Heterogeneities in the Galapagos Mantle Plume. *Geochemistry, Geophysics, Geosystems, 19*(8), 2764-2779. https://doi.org/10.1029/2017GC007338. https://doi.org/10.1029/2017GC007338

Giacomoni, P. P., Bonadiman, C., Casetta, F., Faccini, B., Ferlito, C., Ottolini, L., et al. (2020). Long-term storage of subduction-related volatiles in Northern Victoria Land lithospheric mantle: Insight from olivine-hosted melt inclusions from McMurdo basic lavas (Antarctica). *Lithos, 378-379*, 105826. https://www.sciencedirect.com/science/article/pii/S0024493720304618

Gill, R. & Fitton, G. (2022). *Igneous Rocks and Processes: a Practical Guide;* second edition. John Wiley & Sons. 484 pp.

Guggino, S. N., & Hervig, R. L. (2010). Determination of Fluorine in Fourteen Microanalytical Geologic Reference Materials using SIMS, EPMA, and Proton Induced Gamma Ray Emission (PIGE) Analysis. AGU, Fall meeting V51C-2209.

Guimarães, A. R., Fitton, J. G., Kirstein, L. A., & Barfod, D. N. (2020). Contemporaneous intraplate magmatism on conjugate South Atlantic margins: A hotspot conundrum. *Earth and Planetary Science Letters, 536*, 116147. https://www.sciencedirect.com/science/article/pii/S0012821X2030090X

Guo, M. and Korenaga, J. (2021) A halogen budget of the bulk silicate Earth points to a history of early halogen degassing followed by net regassing. *Proceedings of the National Academy of Sciences*, 118, 51, e2116083118. https://doi.org/10.1073/pnas.2116083118

Hammer, J. E., Coombs, M. L., Shamberger, P. J., & Kimura, J.-I. (2006). Submarine sliver in North Kona: A window into the early magmatic and growth history of Hualalai Volcano, Hawaii. *Journal of Volcanology and*

ORIGINAL UNEDITED MANUSCRIPT

Downloaded from https://academic.oup.com/petrology/advance-article/doi/10.1093/petrology/egad022/7115969 by University of Edinburgh user on 18 April 2023

Geothermal Research, 151(1), 157-188.
https://www.sciencedirect.com/science/article/pii/S0377027305003185

Hanyu, T., Shimizu, K., Ushikubo, T., Kimura, J.-I., Chang, Q., Hamada, M., et al. (2019). Tiny droplets of ocean island basalts unveil Earth's deep chlorine cycle. *Nature Communications, 10*(1), 60.
https://doi.org/10.1038/s41467-018-07955-8

Hartley, M. E., de Hoog, J. C. M., & Shorttle, O. (2021). Boron isotopic signatures of melt inclusions from North Iceland reveal recycled material in the Icelandic mantle source. *Geochimica et Cosmochimica Acta, 294*, 273-294. https://www.sciencedirect.com/science/article/pii/S0016703720306888

Hofmann, A. W. & White, W.M. (1982). Mantle plumes from ancient oceanic crust. *Earth and Planetary Science Letters, 57*, 421-436.

Hirose, K., & Kushiro, I. (1993). Partial melting of dry peridotites at high pressures: Determination of compositions of melts segregated from peridotite using aggregates of diamond. *Earth and Planetary Science Letters*, 114(4), 477-489. https://www.sciencedirect.com/science/article/pii/0012821X9390077M

Honda, M., & Woodhead, J. D. (2005). A primordial solar-neon enriched component in the source of EM-I-type ocean island basalts from the Pitcairn Seamounts, Polynesia. *Earth and Planetary Science Letters, 236*(3), 597-612. https://www.sciencedirect.com/science/article/pii/S0012821X05003766

Humphreys, E. R., & Niu, Y. (2009). On the composition of ocean island basalts (OIB): The effects of lithospheric thickness variation and mantle metasomatism. *Lithos, 112*(1), 118-136.
https://www.sciencedirect.com/science/article/pii/S002449370900187X

Ionov, D. (1998). Trace Element Composition of Mantle-derived Carbonates and Coexisting Phasesin Peridotite Xenoliths from Alkali Basalts. *Journal of Petrology*, 39(11-12), 1931-1941.
https://doi.org/10.1093/petroj/39.11-12.1931

Jackson, M. G., Becker, T. W., & Steinberger, B. (2021). Spatial Characteristics of Recycled and Primordial Reservoirs in the Deep Mantle. *Geochemistry, Geophysics, Geosystems, 22*(3), e2020GC009525.
https://doi.org/10.1029/2020GC009525. https://doi.org/10.1029/2020GC009525

Jochum, K. P., & Stoll, B. (2008). Reference materials for elemental and isotopic analyses by LA-(MC)-ICP-MS: Successes and outstanding needs. *Laser Ablation ICP-MS in the Earth Sciences: Current practices outstanding issues, 40*, 147-168.

John, T., Scambelluri, M., Frische, M., Barnes, J. D., & Bach, W. (2011). Dehydration of subducting serpentinite: Implications for halogen mobility in subduction zones and the deep halogen cycle. *Earth and Planetary Science Letters*, 308(1), 65-76. https://www.sciencedirect.com/science/article/pii/S0012821X11003219

Johnson, L. H., Burgess, R., Turner, G., Milledge, H. J., & Harris, J. W. (2000). Noble gas and halogen geochemistry of mantle fluids: comparison of African and Canadian diamonds. *Geochimica et Cosmochimica Acta*, 64(4), 717-732. https://www.sciencedirect.com/science/article/pii/S0016703799003361

Jones, R. E., De Hoog, J. C. M., Kirstein, L. A., Kasemann, S. A., Hinton, R., Elliott, T., & Litvak, V. D. (2014). Temporal variations in the influence of the subducting slab on Central Andean arc magmas: Evidence from boron isotope systematics. *Earth and Planetary Science Letters, 408*, 390-401.
http://www.sciencedirect.com/science/article/pii/S0012821X14006220

Jones, R. E., Kirstein, L. A., Kasemann, S. A., Dhuime, B., Elliott, T., Litvak, V. D., et al. (2015). Geodynamic controls on the contamination of Cenozoic arc magmas in the southern Central Andes: Insights from the O and

ORIGINAL UNEDITED MANUSCRIPT

Downloaded from https://academic.oup.com/petrology/advance-article/doi/10.1093/petrology/egad022/7115969 by University of Edinburgh user on 18 April 2023

Hf isotopic composition of zircon. *Geochimica et Cosmochimica Acta, 164*, 386-402. http://www.sciencedirect.com/science/article/pii/S0016703715002768

Jørgensen, J. Ø., & Holm, P. M. (2002). Temporal variation and carbonatite contamination in primitive ocean island volcanics from São Vicente, Cape Verde Islands. *Chemical Geology*, 192(3), 249-267. https://www.sciencedirect.com/science/article/pii/S0009254102001985

Kawakatsu, H., P. Kumar, Y. Takei, M. Shinohara, T. Kanazawa, E. Araki, and K. Suyehiro (2009). Seismic evidence for sharp lithosphere asthenosphere boundaries of oceanic plates, *Science*, 324, 499–502, doi:10.1126/science.1169499

Kendrick M.A. (2012). High precision Cl, Br and I determinations in mineral standards using the noble gas method. *Chemical Geology* 292–293, 116–126.

Kendrick, M.A. (2018). Halogens in Seawater, Marine Sediments and the Altered Oceanic Lithosphere. In: Harlov, D., Aranovich, L. (eds) The Role of Halogens in Terrestrial and Extraterrestrial Geochemical Processes. Springer Geochemistry. Springer, Cham. https://doi.org/10.1007/978-3-319-61667-4_9

Kendrick, M. A., Woodhead, J. D., & Kamenetsky, V. S. (2012). Tracking halogens through the subduction cycle. *Geology, 40*(12), 1075-1078. https://doi.org/10.1130/G33265.1B

Kendrick, M. A., Hémond, C., Kamenetsky, V. S., Danyushevsky, L., Devey, C. W., Rodemann, T., et al. (2017). Seawater cycled throughout Earth's mantle in partially serpentinized lithosphere. *Nature Geoscience, 10*(3), 222-228. https://doi.org/10.1038/ngeo2902

Kendrick, M. A., Arculus, R. J., Danyushevsky, L. V., Kamenetsky, V. S., Woodhead, J. D., & Honda, M. (2014). Subduction-related halogens (Cl, Br and I) and H_2O in magmatic glasses from Southwest Pacific Backarc Basins. *Earth and Planetary Science Letters, 400*, 165-176. https://www.sciencedirect.com/science/article/pii/S0012821X14003239

Kendrick, M. A., Caulfield, J. T., Nguyen, A. D., Zhao, J.-x., & Blakey, I. (2020). Halogen and trace element analysis of carbonate-veins and Fe-oxyhydroxide by LA-ICPMS: Implications for seafloor alteration, Atlantis Bank, SW Indian Ridge. *Chemical Geology, 547*, 119668. https://www.sciencedirect.com/science/article/pii/S0009254120302072

Kirstein, L.A., Kelley S, Hawkesworth C, Turner S, Mantovani M, Wijbrans J. (2001). Protracted felsic magmatic activity associated with the opening of the South Atlantic. *Journal of the Geological Society, London, 158*, 583-592.

Kirstein, L. A., Kanev, S., Fitton, J. G., Turner, S. J., & EIMF. (2021). Volcanic spherules condensed from supercritical fluids in the Payenia volcanic province, Argentina. Journal of the Geological Society, 178(1), jgs2020-2026. https://doi.org/10.1144/jgs2020-026

Kiseeva, E. S., Yaxley, G. M., Hermann, J., Litasov, K. D., Rosenthal, A., & Kamenetsky, V. S. (2012). An Experimental Study of Carbonated Eclogite at 3·5–5·5 GPa—Implications for Silicate and Carbonate Metasomatism in the Cratonic Mantle. *Journal of Petrology, 53*(4), 727-759. https://doi.org/10.1093/petrology/egr078

Kobayashi, M., Sumino, H., Burgess, R., Nakai, S. i., Iizuka, T., Nagao, J., et al. (2019). Halogen Heterogeneity in the Lithosphere and Evolution of Mantle Halogen Abundances Inferred From Intraplate Mantle Xenoliths. *Geochemistry, Geophysics, Geosystems*, 20(2), 952-973. https://doi.org/10.1029/2018GC007903.

ORIGINAL UNEDITED MANUSCRIPT

Downloaded from https://academic.oup.com/petrology/advance-article/doi/10.1093/petrology/egad022/7115969 by University of Edinburgh user on 18 April 2023

Kobayashi, M., Sumino, H., Nagao, K., Ishimaru, S., Arai, S., Yoshikawa, M., et al. (2017). Slab-derived halogens and noble gases illuminate closed system processes controlling volatile element transport into the mantle wedge. *Earth and Planetary Science Letters*, 457, 106-116. https://www.sciencedirect.com/science/article/pii/S0012821X16305696

Kobayashi M., Sumino H., Saito T. and Nagao K. (2021) Determination of halogens in geological reference materials using neutron irradiation noble gas mass spectrometry. *Chemical Geology* 582: 120420

Koppers, A. A. P., Becker, T. W., Jackson, M. G., Konrad, K., Müller, R. D., Romanowicz, B., et al. (2021). Mantle plumes and their role in Earth processes. *Nature Reviews Earth & Environment, 2*(6), 382-401. https://doi.org/10.1038/s43017-021-00168-6

Kuritani, T., Xia, Q.-K., Kimura, J.-I., Liu, J., Shimizu, K., Ushikubo, T., et al. (2019). Buoyant hydrous mantle plume from the mantle transition zone. *Scientific Reports, 9*(1), 6549. https://doi.org/10.1038/s41598-019-43103-y

Lesne, P., Kohn, S. C., Blundy, J., Witham, F., Botcharnikov, R. E., & Behrens, H. (2011). Experimental Simulation of Closed-System Degassing in the System Basalt–H2O–CO2–S–Cl. *Journal of Petrology*, 52(9), 1737-1762. https://doi.org/10.1093/petrology/egr027

Matzen, A. K., Baker, M. B., Beckett, J. R., & Stolper, E. M. (2013). The Temperature and Pressure Dependence of Nickel Partitioning between Olivine and Silicate Melt. *Journal of Petrology, 54*(12), 2521-2545. https://doi.org/10.1093/petrology/egt055

Matzen, A., Wood, B., Baker, M. & Stolper, E.M. (2017). The roles of pyroxenite and peridotite in the mantle sources of oceanic basalts. *Nature Geoscience* 10, 530–535. https://doi.org/10.1038/ngeo2968

Mazza, S. E., Gazel, E., Bizimis, M., Moucha, R., Béguelin, P., Johnson, E. A., et al. (2019). Sampling the volatile-rich transition zone beneath Bermuda. *Nature, 569*(7756), 398-403. https://doi.org/10.1038/s41586-019-1183-6

McNamara, A. K. (2019). A review of large low shear velocity provinces and ultra low velocity zones. *Tectonophysics, 760*, 199-220. https://www.sciencedirect.com/science/article/pii/S0040195118301586

Muirhead, J. D., Fischer, T. P., Oliva, S. J., Laizer, A., van Wijk, J., Currie, C. A., et al. (2020). Displaced cratonic mantle concentrates deep carbon during continental rifting. *Nature, 582*(7810), 67-72. https://doi.org/10.1038/s41586-020-2328-3

Mundl, A., Touboul, M., Jackson, M. G., Day, J. M. D., Kurz, M. D., Lekic, V., et al. (2017). Tungsten-182 heterogeneity in modern ocean island basalts. *Science*, 356(6333), 66. http://science.sciencemag.org/content/356/6333/66.abstract

Ni, H., Zhang, L., Xiong, X., Mao, Z., & Wang, J. (2017). Supercritical fluids at subduction zones: Evidence, formation condition, and physicochemical properties. Earth-Science Reviews, 167, 62-71. https://www.sciencedirect.com/science/article/pii/S0012825217300909

Niu, Y. (1997). Mantle Melting and Melt Extraction Processes beneath Ocean Ridges: Evidence from Abyssal Peridotites. *Journal of Petrology, 38*(8), 1047-1074. https://doi.org/10.1093/petroj/38.8.1047

Niu, Y. & O'Hara, M. J. (2008). Global Correlations of Ocean Ridge Basalt Chemistry with Axial Depth: a New Perspective. *Journal of Petrology, 49*(4), 633-664. https://doi.org/10.1093/petrology/egm051

Niu, Y. & Green, D.H. (2018). The petrological control on the lithosphere-asthenosphere boundary (LAB) beneath ocean basins. Earth Science Reviews, 185, 301-306. https://doi.org/10.1016/j.earscirev.2018.06.011

ORIGINAL UNEDITED MANUSCRIPT

Downloaded from https://academic.oup.com/petrology/advance-article/doi/10.1093/petrology/egad022/7115969 by University of Edinburgh user on 18 April 2023

969 Pasyanos, M. E., Masters, T. G., Laske, G., & Ma, Z. (2014). LITHO1.0: An updated crust and lithospheric model
970 of the Earth. *Journal of Geophysical Research: Solid Earth, 119*(3), 2153-2173.
971 https://doi.org/10.1002/2013JB010626

972 Pearson, D. G., Brenker, F. E., Nestola, F., McNeill, J., Nasdala, L., Hutchison, M. T., et al. (2014). Hydrous
973 mantle transition zone indicated by ringwoodite included within diamond. *Nature, 507*(7491), 221-224.
974 https://doi.org/10.1038/nature13080

975 Prytulak, J., & Elliott, T. (2007). TiO2 enrichment in ocean island basalts. *Earth and Planetary Science Letters,*
976 *263*(3), 388-403. https://www.sciencedirect.com/science/article/pii/S0012821X07005936

977 Rasmussen, D. J., Plank, T. A., Wallace, P. J., Newcombe, M. E., & Lowenstern, J. B. (2020). Vapor-bubble
978 growth in olivine-hosted melt inclusions. *American Mineralogist*, 105(12), 1898-1919.
979 https://doi.org/10.2138/am-2020-7377

980 Roddick, J. C. (1983). High precision intercalibration of 40Ar-39Ar standards. *Geochimica et Cosmochimica Acta*,
981 47, 887–898.

982 Ruzié-Hamilton, L., Clay, P.L., Burgess, R., Joachim, B., Ballentine, C.J., and Turner, G. (2016) Determination of
983 halogen abundances in terrestrial and extraterrestrial samples by the analysis of noble gases produced by
984 neutron irradiation. *Chemical Geology* 437, 77–87.

985 Savov, I. P., Ryan, J. G, D'Antonio, M., Fryer, P., 2007. Shallow slab fluid release across and along the Mariana
986 arc-basin system: Insights from geochemistry of serpentinized peridotites from the Mariana Forearc, *Journal of*
987 *Geophysical Research*, doi:10.1029/2006JB004749.

988 Sisson, T. W., Kimura, J. I., & Coombs, M. L. (2009). Basanite–nephelinite suite from early Kilauea: carbonated
989 melts of phlogopite–garnet peridotite at Hawaii's leading magmatic edge. *Contributions to Mineralogy and*
990 *Petrology, 158*(6), 803. https://doi.org/10.1007/s00410-009-0411-8

991 Smith, E. M., Shirey, S. B., Richardson, S. H., Nestola, F., Bullock, E. S., Wang, J., & Wang, W. (2018). Blue boron-
992 bearing diamonds from Earth's lower mantle. *Nature, 560*(7716), 84-87. https://doi.org/10.1038/s41586-018-
993 0334-5

994 Snyder, G.T., Savov, I. P., Muramatsu, Y., 2004. Iodine and boron in Mariana serpentine mud volcanoes (ODP
995 125 and 195): Implications for forearc processes and subduction recycling, In Shinohara, M., Salisbury, M.H.,
996 and Richter, C. (Eds.), Proc. ODP, Sci. Results, 195.

997 Sobolev, A. V., Hofmann, A. W., Kuzmin, D. V., Yaxley, G. M., Arndt, N. T., Chung, S.-L., et al. (2007). The
998 Amount of Recycled Crust in Sources of Mantle-Derived Melts. *Science*, 316(5823), 412.

999 Spice, H. E., Fitton, J. G., & Kirstein, L. A. (2016). Temperature fluctuation of the Iceland mantle plume through
1000 time. *Geochemistry, Geophysics, Geosystems, 17*(2), 243-254. https://doi.org/10.1002/2015GC006059.
1001 https://doi.org/10.1002/2015GC006059

1002 Stroncik, N. A., & Haase, K. M. (2004). Chlorine in oceanic intraplate basalts: Constraints on mantle sources and
1003 recycling processes. *Geology, 32*(11), 945-948.

1004 Stoffers, P., & Hékinian, R. (1990). *Cruise Report SONNE 65-Midplate II, Hot Spot Volcanism in the Central*
1005 *Southpacific*: Geologisch-Paläontologisches Institut und Museum Christian-Albrechts. 40, 233.

1006 Sumino, H., Burgess, R., Mizukami, T., Wallis, S. R., Holland, G., & Ballentine, C. J. (2010). Seawater-derived
1007 noble gases and halogens preserved in exhumed mantle wedge peridotite. Earth and Planetary Science Letters,
1008 294(1), 163-172.

ORIGINAL UNEDITED MANUSCRIPT

Downloaded from https://academic.oup.com/petrology/advance-article/doi/10.1093/petrology/egad022/7115969 by University of Edinburgh user on 18 April 2023

Taracsák, Z., Hartley, M. E., Burgess, R., Edmonds, M., Iddon, F., & Longpré, M. A. (2019). High fluxes of deep volatiles from ocean island volcanoes: Insights from El Hierro, Canary Islands. *Geochimica et Cosmochimica Acta, 258*, 19-36. https://www.sciencedirect.com/science/article/pii/S001670371930287X

Torsvik, T. H., Steinberger, B., Cocks, L. R. M., & Burke, K. (2008). Longitude: Linking Earth's ancient surface to its deep interior. *Earth and Planetary Science Letters, 276*(3), 273-282. https://www.sciencedirect.com/science/article/pii/S0012821X08006328

Tsekhmistrenko, M., Sigloch, K., Hosseini, K., & Barruol, G. (2021). A tree of Indo-African mantle plumes imaged by seismic tomography. Nature Geoscience, 14(8), 612-619. https://doi.org/10.1038/s41561-021-00762-9

Urann, B. M., Le Roux, V., Hammond, K., Marschall, H. R., Lee, C. T. A., & Monteleone, B. D. (2017). Fluorine and chlorine in mantle minerals and the halogen budget of the Earth's mantle. *Contributions to Mineralogy and Petrology, 172*(7), 51. https://doi.org/10.1007/s00410-017-1368-7

Valer, M., Bachèlery, P., & Schiano, P. (2017). The Petrogenesis of Plagioclase-ultraphyric Basalts from La Réunion Island. *Journal of Petrology, 58*(4), 675-698. https://doi.org/10.1093/petrology/egx030

van Acken, D., Becker, H., Hammerschmidt, K., Walker, R. J., & Wombacher, F. (2010). Highly siderophile elements and Sr–Nd isotopes in refertilized mantle peridotites — A case study from the Totalp ultramafic body, Swiss Alps. *Chemical Geology, 276*(3), 257-268. https://www.sciencedirect.com/science/article/pii/S0009254110002226

Walowski, K. J., Kirstein, L. A., De Hoog, J. C. M., Elliott, T. R., Savov, I. P., & Jones, R. E. (2019). Investigating ocean island mantle source heterogeneity with boron isotopes in melt inclusions. *Earth and Planetary Science Letters, 508*, 97-108. http://www.sciencedirect.com/science/article/pii/S0012821X18307143

Walowski, K. J., Kirstein, L. A., De Hoog, J. C. M., Elliott, T., Savov, I. P., Jones, R. E., & Eimf. (2021). Boron recycling in the mantle: Evidence from a global comparison of ocean island basalts. *Geochimica et Cosmochimica Acta, 302*, 83-100. https://www.sciencedirect.com/science/article/pii/S0016703721001812

Walowski, K. J., Wallace, P. J., Clynne, M. A., Rasmussen, D. J., & Weis, D. (2016). Slab melting and magma formation beneath the southern Cascade arc. *Earth and Planetary Science Letters*, 446, 100-112. https://www.sciencedirect.com/science/article/pii/S0012821X1630139X

Wang, W., Liu, J., Zhu, F., Li, M., Dorfman, S. M., Li, J., & Wu, Z. (2021). Formation of large low shear velocity provinces through the decomposition of oxidized mantle. *Nature Communications, 12*(1), 1911. https://doi.org/10.1038/s41467-021-22185-1

Wang, X.-J., Chen, L.-H., Hofmann, A. W., Mao, F.-G., Liu, J.-Q., Zhong, Y., et al. (2017). Mantle transition zone-derived EM1 component beneath NE China: Geochemical evidence from Cenozoic potassic basalts. *Earth and Planetary Science Letters, 465*, 16-28. https://www.sciencedirect.com/science/article/pii/S0012821X17300961

Weiss, Y., Class, C., Goldstein, S. L., & Hanyu, T. (2016). Key new pieces of the HIMU puzzle from olivines and diamond inclusions. *Nature, 537*(7622), 666-670. https://doi.org/10.1038/nature19113

White, W. M. (2015). Probing the Earth's deep interior through geochemistry. *Geochemical Perspectives, 4*(2), 95-251.

Williams, Q., & Garnero, E. J. (1996). Seismic Evidence for Partial Melt at the Base of Earth's Mantle. *Science, 273*(5281), 1528. http://science.sciencemag.org/content/273/5281/1528.abstract

ORIGINAL UNEDITED MANUSCRIPT

Downloaded from https://academic.oup.com/petrology/advance-article/doi/10.1093/petrology/egad022/7115969 by University of Edinburgh user on 18 April 2023

1047 Woodhead, J. D., & McCulloch, M. T. (1989). Ancient seafloor signals in Pitcairn Island lavas and evidence for
1048 large amplitude, small length-scale mantle heterogeneities. *Earth and Planetary Science Letters, 94*(3), 257-
1049 273. https://www.sciencedirect.com/science/article/pii/0012821X89901453

1050 Woodhead, J. D., & Devey, C. W. (1993). Geochemistry of the Pitcairn seamounts, I: source character and
1051 temporal trends. *Earth and Planetary Science Letters, 116*(1), 81-99.
1052 https://www.sciencedirect.com/science/article/pii/0012821X9390046C

1053 Wyllie, P. J. (1988). Magma genesis, plate tectonics, and chemical differentiation of the Earth. *Reviews of*
1054 *Geophysics, 26*(3), 370-404. https://doi.org/10.1029/RG026i003p00370.
1055 https://doi.org/10.1029/RG026i003p00370

1056 Yoder, H.S. & Tilley, C.E. (1962) Origin of Basalt Magmas: An Experimental Study of Natural and Synthetic Rock
1057 Systems. Journal of Petrology, 3, 342-532. http://dx.doi.org/10.1093/petrology/3.3.342

1058

ORIGINAL UNEDITED MANUSCRIPT

Downloaded from https://academic.oup.com/petrology/advance-article/doi/10.1093/petrology/egad022/7115969 by University of Edinburgh user on 18 April 2023

1059

1060 Table 1. Summary information for analysed ocean island basalt samples.

Ocean island	Lithospheric thickness (km)	Eruption	Plume type	Glass	Olivine/Melt inclusions	EPMA	SIMS	NI-NGMS
Ascension	39.6	Subaerial	EM/HIMU	*		*	*	
Fogo	68.9	Subaerial	EM/HIMU	*	*	*	*	^
La Palma	53.6	Subaerial	HIMU					
LP1002				*	*	*	*	*
LP1017					*	*	*	*
LP1025					*	*	*	*
Xenolith								*
La Réunion	60.2	Subaerial	EM		*	*	*	*
MacDonald	51.7	Submarine	EM/HIMU	*	*	*	*	*
Pitcairn	50.0	Submarine	EM					
51DS-2				*	*	*	*	*
55-SLS				*	*	*	*	*
St. Helena	54.0	Submarine	HIMU	*		*	*	~
Tristan da Cunha	42.8	Subaerial	EM	*		*	*	

1061 La Palma localities: Barranco Fagundo (LP1002); Holocene cone (LP1017); Tephra 1949 eruption Vólcan
1062 Duraznero (LP1025). Cape Verdes, Pico do Fogo localities include tephra from eruptions dated to 1816, 1951
1063 and 1995. Pitcairn islands: Volcano 2 (51DS-2) and Volcano 5 (55-SLS). La Réunion: Piton de Caille vent. EM –
1064 enriched mantle; HIMU – high time integrated U/Pb (μ). Electron probe microanalysis (EPMA); Secondary
1065 ionisation mass sprectrometry (SIMS); Neutron-irradiation noble gas mass spectrometry (NI-NGMS): olivine
1066 analysed except for localities indicated by ^ (both glass and olivine) and ~ (glass only).

1067

ORIGINAL UNEDITED MANUSCRIPT

Downloaded from https://academic.oup.com/petrology/advance-article/doi/10.1093/petrology/egad022/7115969 by University of Edinburgh user on 18 April 2023

1068

1069 Table 2. Average olivine compositional data for selected ocean island basalts.

	Al_2O_3	SiO_2	CaO	FeO	Na_2O	MgO	P_2O_5	MnO	NiO	Fo*
La Palma										
LP1017	0.05	39.06	0.31	16.38	0.01	43.39	0.03	0.22	0.23	82.01
LP1025	0.05	38.84	0.25	18.06	0.01	43.18	0.02	0.24	0.18	80.68
LP1002	0.05	39.30	0.26	14.40	0.01	46.00	0.01	0.19	0.29	84.60
LP1006	0.03	38.38	0.20	20.80	0.01	40.82	0.03	0.29	0.14	77.31
Ascension										
MI01	0.05	37.58	0.23	24.34	0.01	38.19	0.04	0.30	0.07	73.19
Fogo										
K-FG03	0.03	38.80	0.31	17.84	0.01	41.67	0.02	0.27	0.10	79.79
La Réunion										
RPC	0.07	39.69	0.21	13.76	0.01	46.08	0.01	0.17	0.39	85.26
Pitcairn										
51DS22	0.07	39.38	0.29	14.27	0.01	45.82	0.01	0.19	0.24	84.63
55SLS	0.05	38.92	0.21	18.14	0.00	42.74	0.02	0.22	0.25	80.35
51DS21	0.05	39.26	0.21	16.5	0.01	44.01	0.04	0.20	0.26	82.22
MacDonald										
110DS	0.06	38.93	0.21	16.51	0.01	44.09	0.03	0.20	0.27	82.24

1070 *Fo = atomic Mg/(Mg+Fe)*100

1071

ORIGINAL UNEDITED MANUSCRIPT

Downloaded from https://academic.oup.com/petrology/advance-article/doi/10.1093/petrology/egad022/7115969 by University of Edinburgh user on 18 April 2023

1072 Table 3. Halogen data in molar ratios of glass and olivine separates measured using neutron-irradiation noble
1073 gas mass spectrometry. FAG-X denotes xenolith olivine.

Sample	K/Cl	±K/Cl	Br/Cl	±Br/Cl	I/Cl	±I/Cl	Cl (ppm)
Glass							
Fogo							
K-FG-10g	24.98	0.46	1.04E-03	1.10E-04	6.47E-06	5.06E-07	1023
K-FG-10g	24.06	0.44	2.20E-03	2.32E-04	2.24E-05	1.80E-06	44
K-FG-10	24.62	0.28	1.28E-03	1.25E-04	9.60E-06	7.41E-07	1196
K-FG-10	24.58	0.28	1.25E-03	1.21E-04	8.80E-06	6.73E-07	1170
K-FG-10	24.74	0.28	1.18E-03	1.15E-04	7.62E-06	5.86E-07	1201
K-FG-03	28.18	0.32	1.33E-03	1.30E-04	1.03E-05	8.04E-07	795
K-FG-03	28.17	0.32	1.39E-03	1.35E-04	1.04E-05	7.94E-07	932
K-FG-08g	32.91	0.61	1.05E-03	1.11E-04	1.08E-05	8.54E-07	514
K-FG-08g	62.06	1.17	7.28E-04	7.68E-05	2.18E-05	1.96E-06	0.7
K-FG-08g	31.40	0.38	1.34E-03	1.31E-04	1.24E-05	1.14E-06	97
K-FG-08g	30.26	0.34	1.32E-03	1.28E-04	1.23E-05	9.32E-07	564
K-FG-08g	31.45	0.35	1.35E-03	1.31E-04	1.25E-05	9.82E-07	738
St Helena							
SO84-16DS	13.67	0.26	9.71E-04	1.03E-04	7.37E-06	5.88E-07	255
Olivine							
Fogo							
K-FG-10g	26.54	0.54	1.27E-03	1.39E-04	2.57E-05	2.11E-06	6.8
K-FG-10g	25.04	0.47	9.63E-04	1.02E-04	8.22E-06	6.44E-07	1083
K-FG-10g	26.05	0.50	1.11E-03	1.17E-04	4.09E-05	3.49E-06	7.8
K-FG-03	26.91	0.50	1.27E-03	1.36E-04	1.03E-05	8.64E-07	15.1
K-FG-03	15.76	2.55	3.52E-03	3.80E-04	1.08E-04	1.33E-05	14
K-FG-03	28.38	30.70	2.06E-03	6.33E-03	2.93E-05	5.21E-05	42
K-FG-08	29.03	0.56	1.07E-03	1.13E-04	1.25E-05	1.08E-06	20.2
La Palma							
LP-16-1017	19.68	1.16	9.41E-04	3.28E-04	9.58E-06	2.47E-06	0.86
LP-16-1025	45.00	1.00	9.21E-04	1.02E-04	8.87E-05	7.94E-06	1.94
LP-16-1002	21.16	0.40	1.06E-03	1.12E-04	1.07E-04	8.53E-06	14.5
FAG-X-01b	20.44	2.37	1.64E-03	2.22E-04	7.72E-05	9.04E-06	0.8
FAG-X-01b	25.34	0.76	1.58E-03	1.73E-04	1.31E-04	1.06E-05	1.97
FAG-X-04a	81.74	31.65			5.80E-04	6.60E-05	0.04
Pitcairn							
55-SLS-1g	19.92	0.37	1.10E-03	1.17E-04	1.06E-05	8.41E-07	582
SO65-51DS	28.12	0.52	1.08E-03	1.14E-04	1.93E-05	1.52E-06	270
SO65-51DS	27.50	0.64	1.23E-03	1.32E-04	3.79E-05	3.65E-06	1.75
La Reunion							
Reunion 1	35.67	8.57	1.73E-03	3.19E-04	5.13E-05	2.24E-05	0.2
ReU-MS-16	33.19	0.62	8.51E-04	8.98E-05	7.06E-06	5.60E-07	176
MacDonald							
110-DS-4	19.67	0.37	9.06E-04	9.57E-05	1.46E-05	1.15E-06	434

ORIGINAL UNEDITED MANUSCRIPT

Downloaded from https://academic.oup.com/petrology/advance-article/doi/10.1093/petrology/egad022/7115969 by University of Edinburgh user on 18 April 2023

Figure captions

Figure 1. Distribution of ocean island basalt samples used in this study; new data, filled squares; published data, open squares. 1. La Réunion; 2. Tristan da Cunha; 3. St. Helena; 4. Ascension; 5. Cape Verdes (Fogo); 6. Canary Islands (La Palma); 7. MacDonald (Ra) seamount; 8. Pitcairn; 9. Cook Islands; 10. Hawai'i; 11. Iceland; 12. Canary Islands (Terceira).

Figure 2. Olivine compositional data from a range of ocean island basalt localities. Left panel shows new data, right panel published olivine compositional data from a range of plume-related intraplate magmatism. Published data from Iceland 1, North Atlantic igneous province (NAIP), Greenland, Baffin Island (Spice et al., 2015); Iceland 2, Hawai'i (Sobolev et al., 2007); Cook islands (Weiss et al., 2016). Analytical error is less than symbol size. Pyroxenite and peridotite labels in 2e reflect range of Ni/Mg and Mn/Fe in olivine derived from melting of those sources after Sobolev et al. (2007).

Figure 3. Plot of heavy halogen ratios, I/Cl versus Br/Cl, from olivine, glass and xenolith analyses of OIB and xenolith samples generated using neutron-irradiation noble gas mass spectrometry. Fields for MORB, serpentinites, marine pore fluids and diamonds included for comparison. Data from this study and from Johnson et al. (2000); Burgess et al. (2002).

Figure 4. (a) Silica saturation index (SSI) plotted against incompatible-element ratio Nb/Zr highlighting large variability in glass compositional data that is unrelated to low-pressure fractional crystallisation. Critical plane of silica saturation separates silica-saturated (above) from undersaturated (below) compositions. Fogo glass samples have remarkably low SSI and high Nb/Zr indicating that they represent the smallest-degree melts from a particularly enriched source. The presence of carbonate in the source region drives melts to lower SSI. Melting of pyroxenite drives SSI to positive values. Published datasets from Hawai'i (Hammar et al., 2006; Dixon et al., 2008; Sisson et al., 2009; Garcia et al., 2016); Iceland (Hartley et al., 2021); Canary Island (El Hiero) (Taracsák et al., 2019). Samples from Hawai'i are divided according to island and proposed source variability (e.g. Niihau, has a carbonated eclogite component in the source; Dixon et al., 2008). Analytical error is less than symbol size.

(b) Plot of lithospheric thickness estimated using LITHO 1.0 (Pasyanos et al., 2014) versus Nb/Zr highlighting the lack of correlation between degree of melting and lithospheric lid thickness in these OIB. This suggests that the onset of melting is determined more by mantle temperature and volatile content than by lithosphere thickness. There is no systematic difference between the composition of glass and melt inclusions.

Figure 5. (a) Positive correlation between F (ppm) and Ce/Y. Note Tristan samples are the only OIB that plot off the trend at high Ce/Y but relatively low F (ppm). Correlation suggests F is behaving incompatibly. Analytical error is less than symbol size.

(b) Cl versus Nb/Zr for glass and melt inclusion data indicating distinctively different compositions from Pitcairn and La Réunion compared with the other OIB analyses. La Palma melt inclusions: H, Holocene cone LP1017; VD, Vólcan Duraznero LP1025; BF1, Barranco Fagundo 01; BF2, Barranco Fagundo 02.

Figure 6. (a) Nb/Zr versus silica saturation index (SSI) for melt inclusion and glass data. Curves are for decompression melting of fertile peridotite (HK66) with potential temperatures of 1300°C (blue), 1400°C (green), 1500°C (red) based on the experimental work of Hirose and Kushiro (1993) and the melting model of Fitton et al. (2021). Note that only samples from Fogo can potentially be derived from a peridotite source. (b) Silica saturation index (SSI) plotted against F (ppm) for melt inclusions, which should not suffer volatile loss in the same way as glass. Analytical error is less than symbol size.

ORIGINAL UNEDITED MANUSCRIPT

Downloaded from https://academic.oup.com/petrology/advance-article/doi/10.1093/petrology/egad022/7115969 by University of Edinburgh user on 18 April 2023

Figure 7. (a) Cl/K versus Cl/Nb ratios for OIB including fields for the Cook-Austral HIMU islands (Hanyu et al., 2019) and MORB showing distinctively different geochemical reservoir signatures for HIMU and EM. Dehydration of altered oceanic crust and loss of both Cl and K, which may be linked to slab age, appears to control the HIMU trend. Cl/Nb variability is linked to carbonate component. (b) F/Zr versus Cl/Nb shows a clear difference in F between subalkali OIB such as La Réunion and Pitcairn and the other OIB which have HIMU-like components. Mantle domain labels are from the literature (Table 1; Escrig et al., 2005; Walowski et al., 2019; 2021). These melt inclusions may have degassed; however, Cl degasses at greater depth than F, which suggests that the difference reflects source variability. Analytical error is less than symbol size.

Figure 8. (a) Fluorine versus TiO_2 wt.%; (b) Cl versus TiO_2 wt.% showing variable enrichment in F and Cl for different OIB. Dashed lines are different F/TiO_2 and Cl/TiO_2 respectively reflecting relative enrichment in F and Cl. Hawai'i data (Sisson et al., 2009) show shallow-level degassing of F in shield stage magmatism. Data suggest different end members have variable fluorine and other halogen components, which may be dominated by altered, carbonated subducted oceanic crust. Analytical error is less than symbol size.

Figure 9. Schematic model of a section through the Earth showing potential heterogeneity introduced as a function of material cycling. Ocean island basalt- OIB; Mid ocean ridge basalt – MORB. Subducting oceanic crust and lithosphere varies in its age and degree of alteration, progressively releasing volatiles and other elements at various depths through dehydration reactions. Break-up of the subducting slabs may occur at a variety of levels, some may penetrate to the lowermost mantle. White arrows represent C-O-H rich fluids; black arrows dehydration reactions; both lead to metasomatism of the mantle. Black curved lines represent area potentially affected by rising thermochemical plume and highlights potential to entrain heterogeneous components.

ORIGINAL UNEDITED MANUSCRIPT

Downloaded from https://academic.oup.com/petrology/advance-article/doi/10.1093/petrology/egad022/7115969 by University of Edinburgh user on 18 April 2023

Fig. 1.

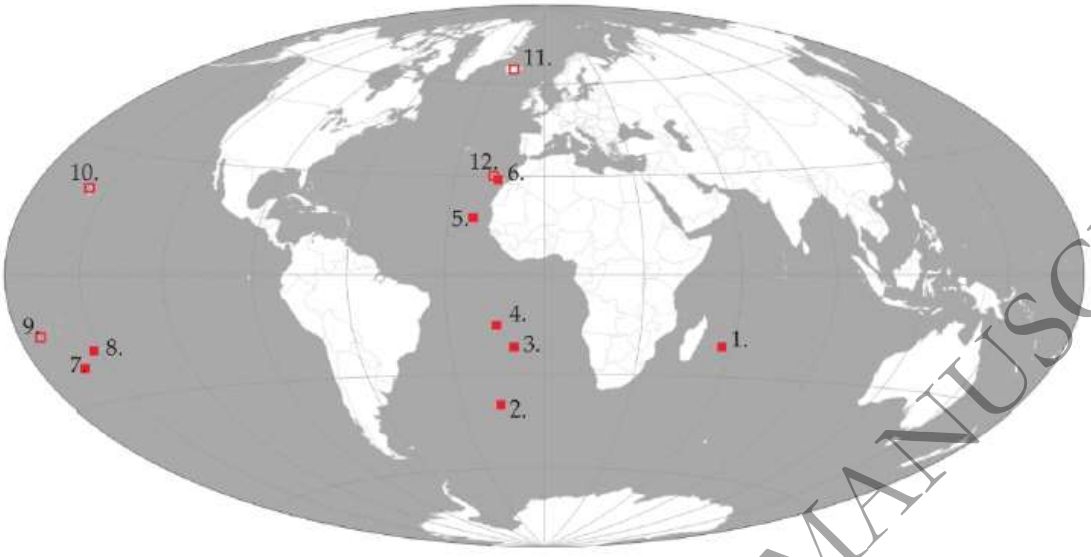

ORIGINAL UNEDITED MANUSCRIPT

Downloaded from https://academic.oup.com/petrology/advance-article/doi/10.1093/petrology/egad022/7115969 by University of Edinburgh user on 18 April 2023

1157 **Fig. 2.**

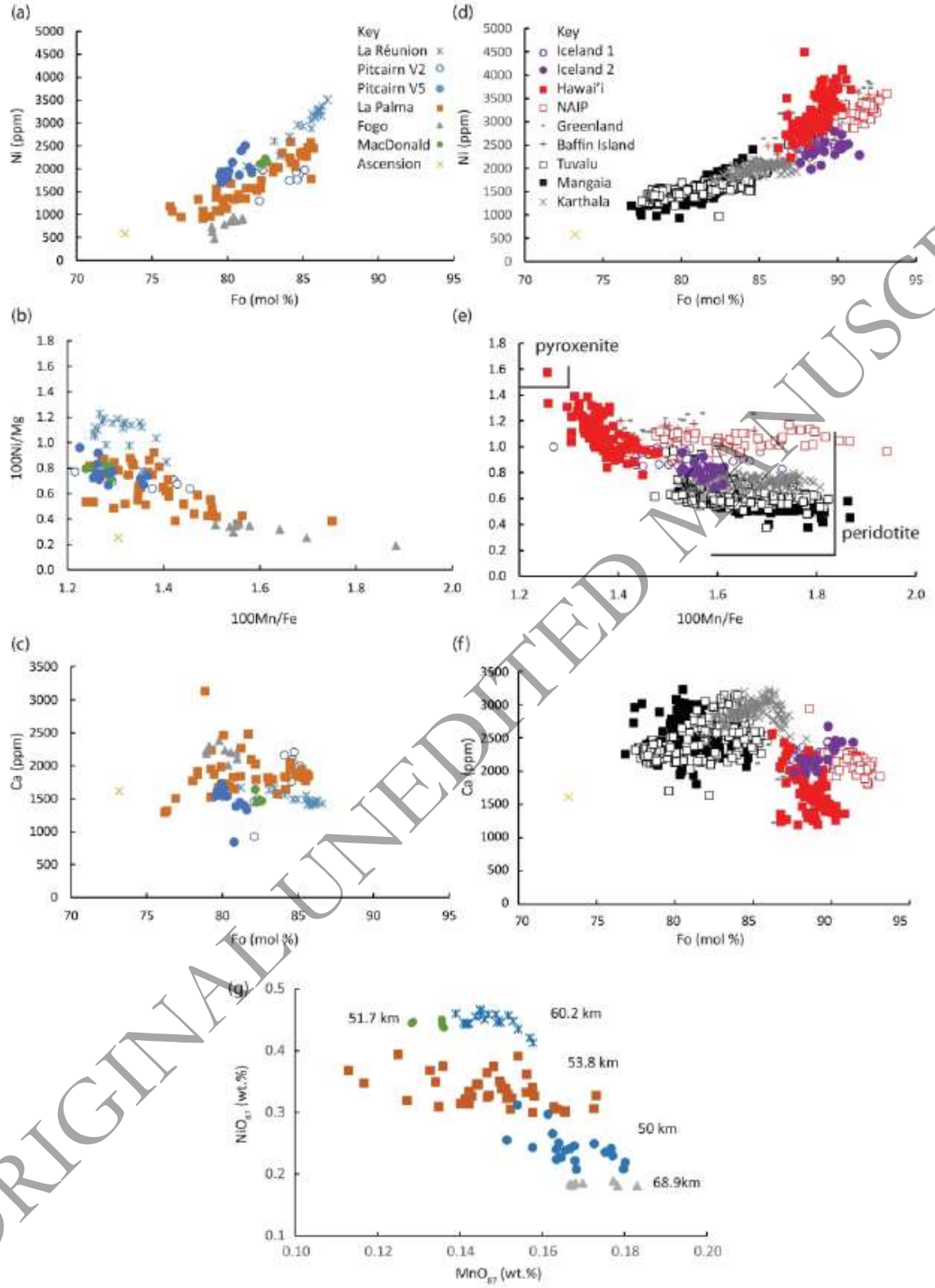

1158

1159

1160

ORIGINAL UNEDITED MANUSCRIPT

Downloaded from https://academic.oup.com/petrology/advance-article/doi/10.1093/petrology/egad022/7115969 by University of Edinburgh user on 18 April 2023

Fig. 3.

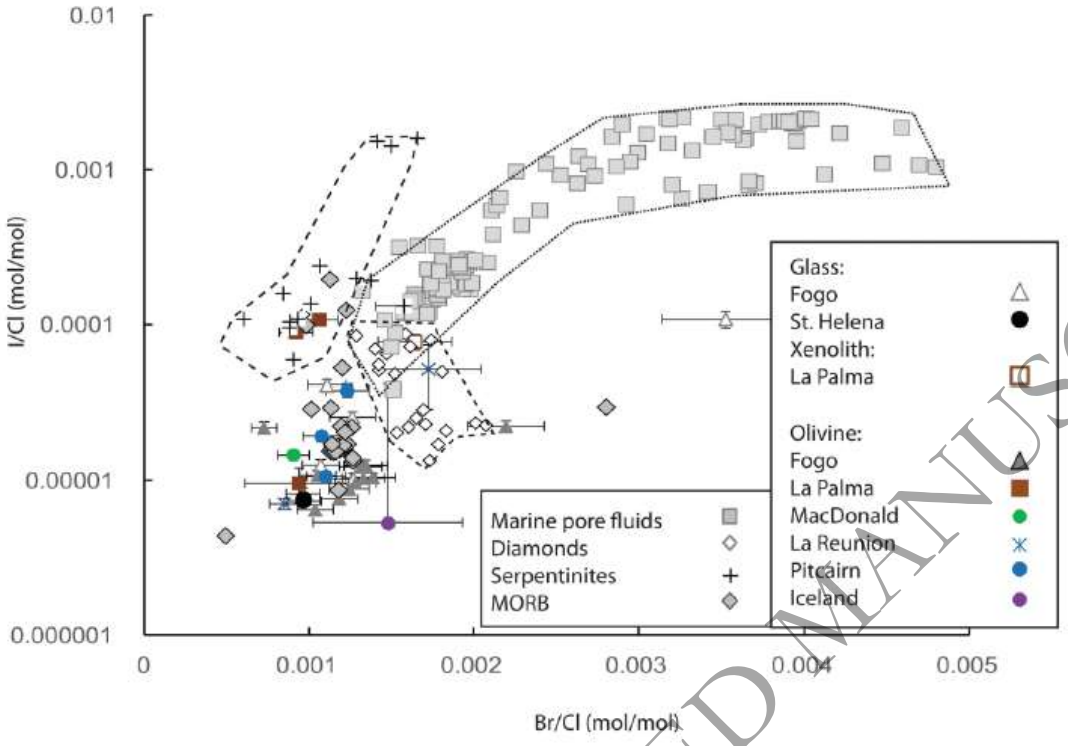

ORIGINAL UNEDITED MANUSCRIPT

Downloaded from https://academic.oup.com/petrology/advance-article/doi/10.1093/petrology/egad022/7115969 by University of Edinburgh user on 18 April 2023

Fig. 4.

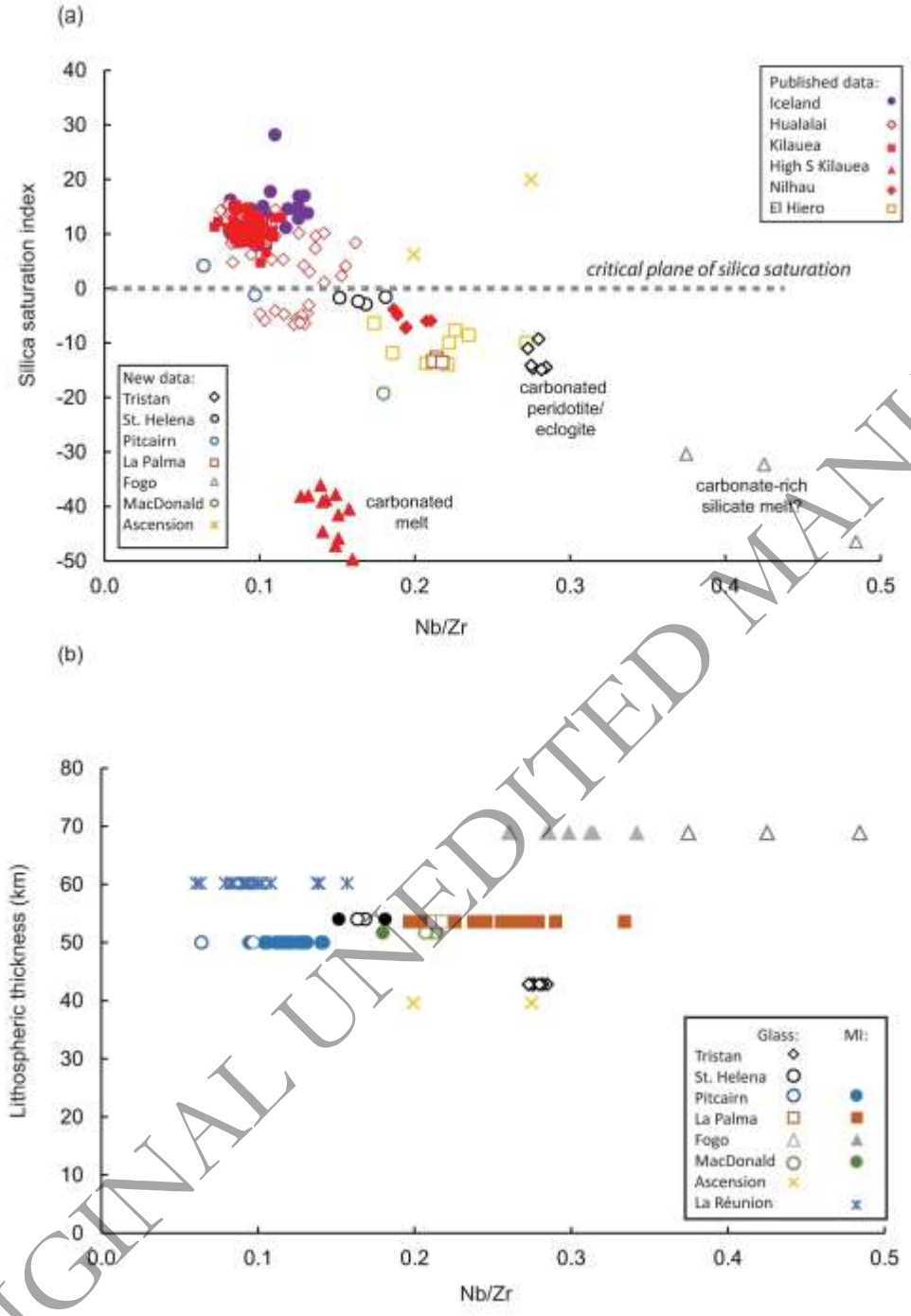

ORIGINAL UNEDITED MANUSCRIPT

Downloaded from https://academic.oup.com/petrology/advance-article/doi/10.1093/petrology/egad022/7115969 by University of Edinburgh user on 18 April 2023

1186 **Fig. 5.**

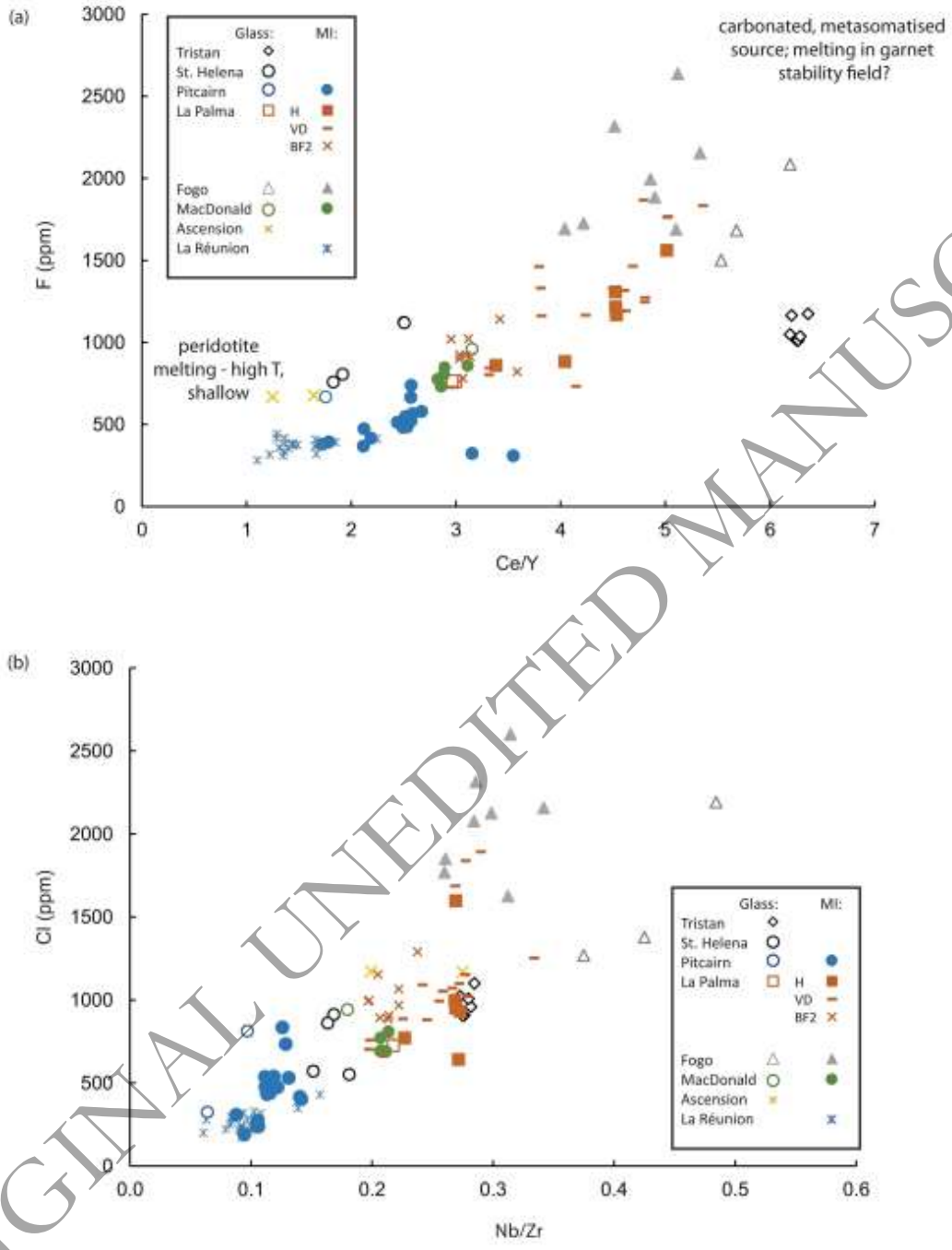

1187

1188

1189

1190

1191

1192

ORIGINAL UNEDITED MANUSCRIPT

Downloaded from https://academic.oup.com/petrology/advance-article/doi/10.1093/petrology/egad022/7115969 by University of Edinburgh user on 18 April 2023

Fig. 6.

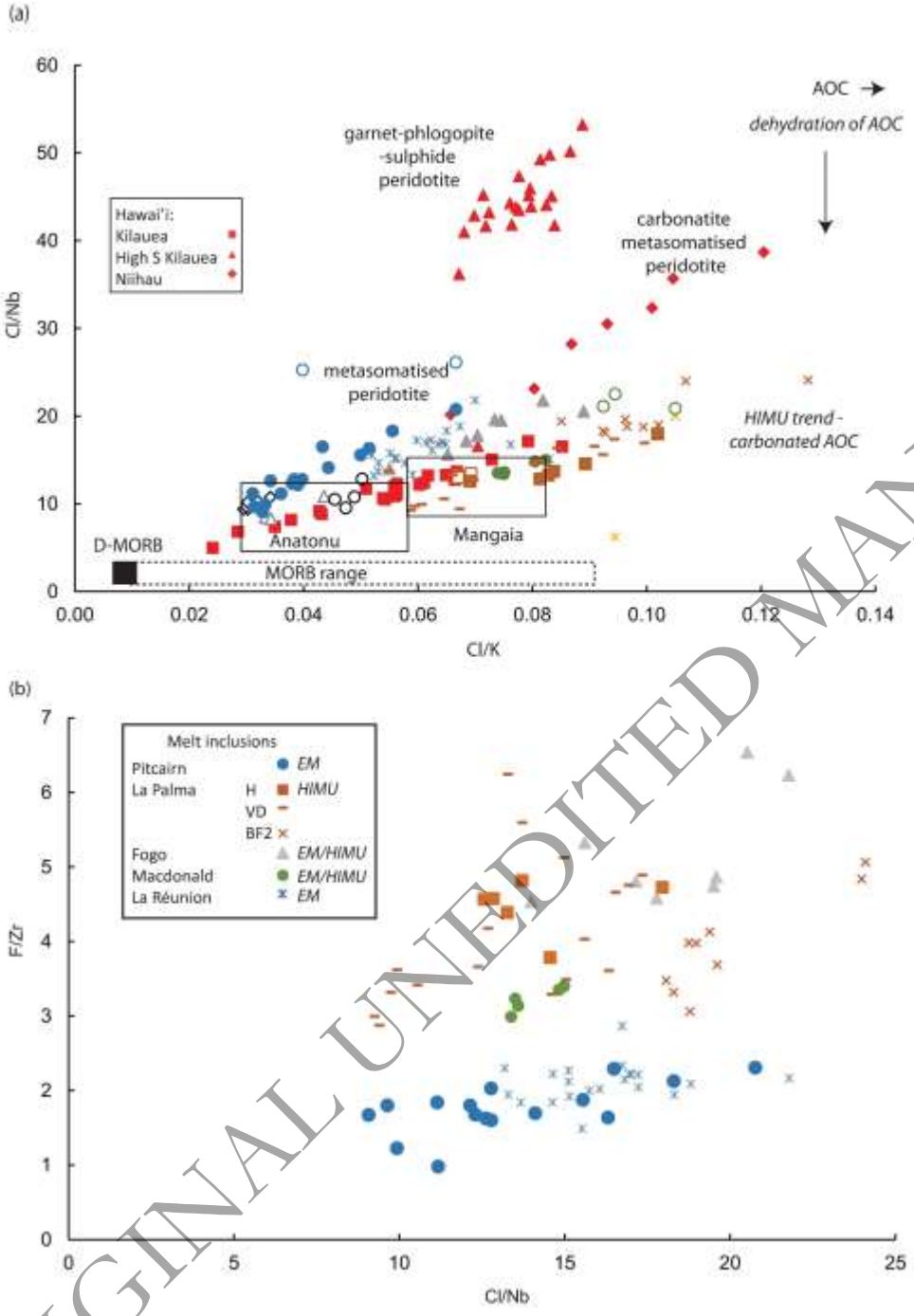

ORIGINAL UNEDITED MANUSCRIPT

Downloaded from https://academic.oup.com/petrology/advance-article/doi/10.1093/petrology/egad022/7115969 by University of Edinburgh user on 18 April 2023

1201 **Fig. 7.**

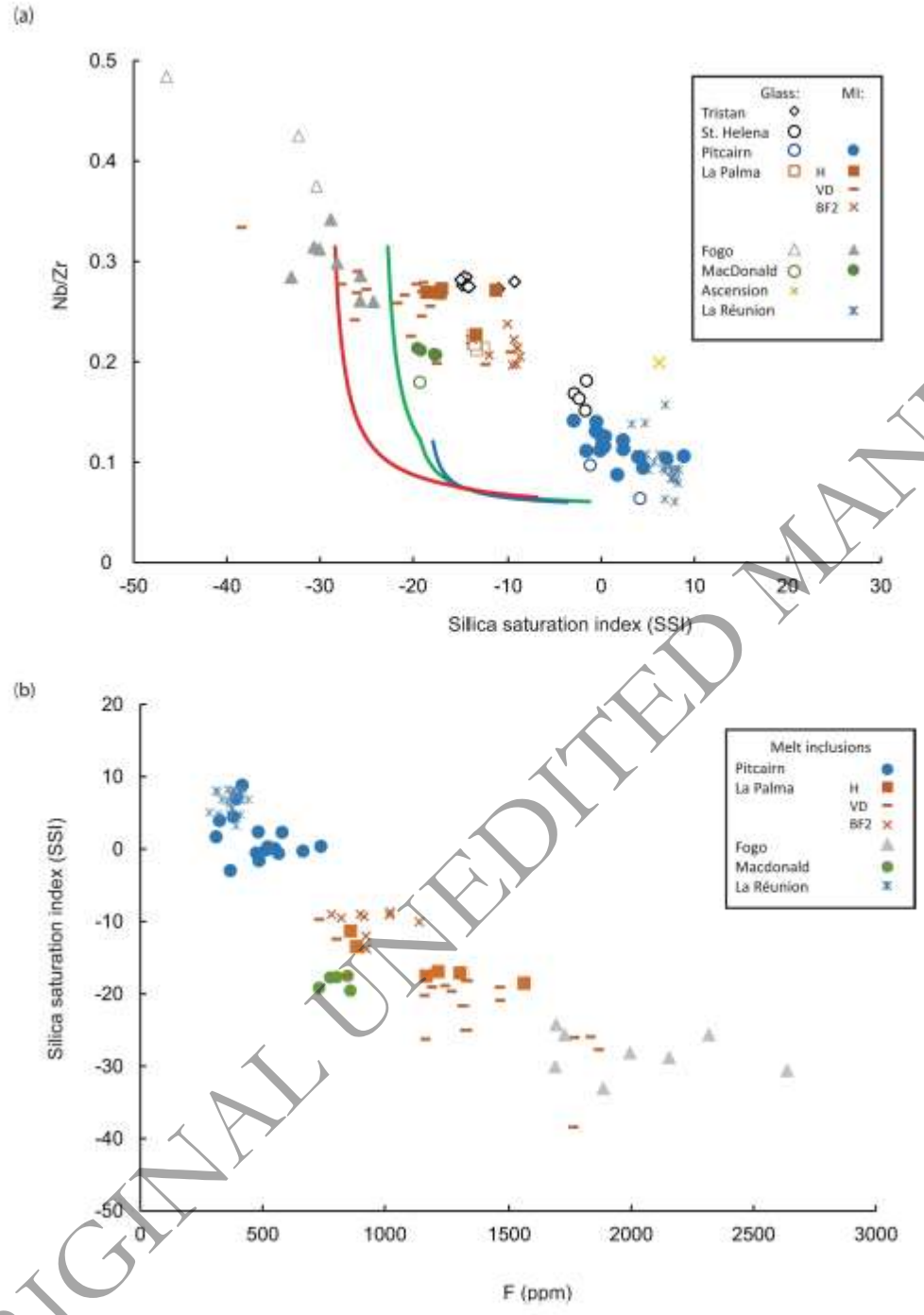

1202
1203
1204
1205
1206
1207

ORIGINAL UNEDITED MANUSCRIPT

Downloaded from https://academic.oup.com/petrology/advance-article/doi/10.1093/petrology/egad022/7115969 by University of Edinburgh user on 18 April 2023

1208 **Fig. 8.**

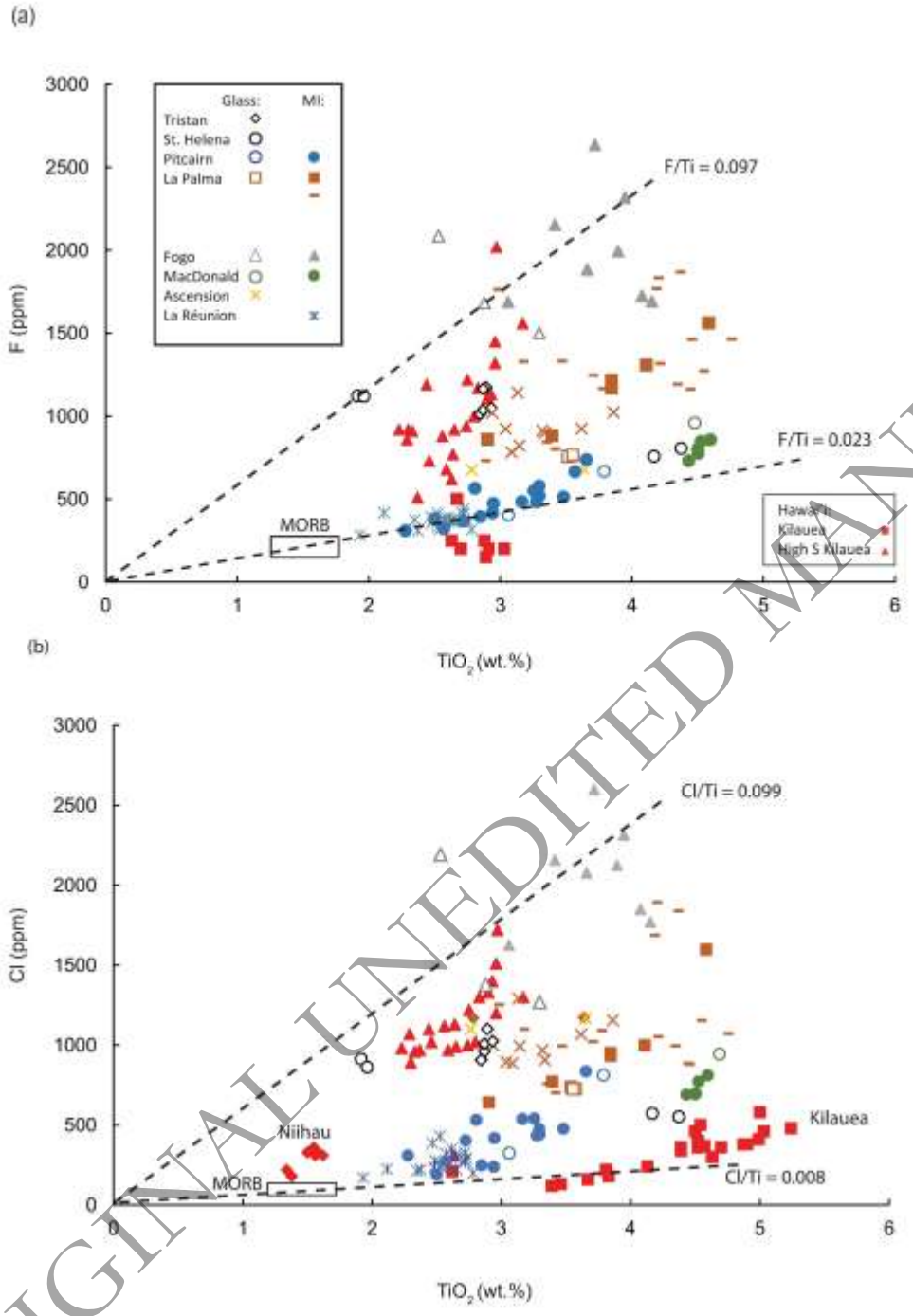

1209

1210

1211

1212

1213

1214

ORIGINAL UNEDITED MANUSCRIPT

Downloaded from https://academic.oup.com/petrology/advance-article/doi/10.1093/petrology/egad022/7115969 by University of Edinburgh user on 18 April 2023

1215 **Fig. 9.**

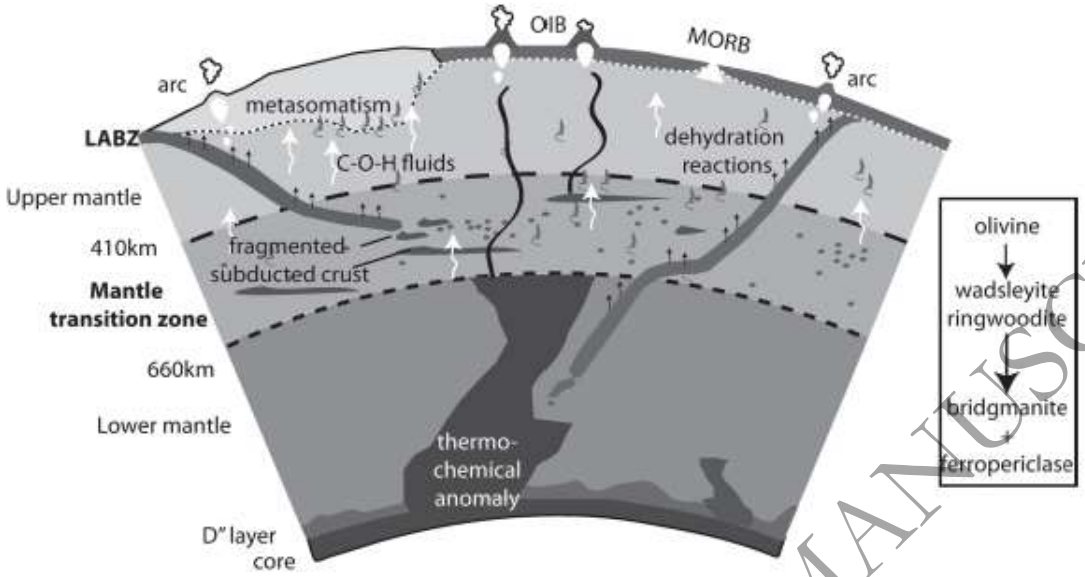

1216

ORIGINAL UNEDITED MANUSCRIPT

Downloaded from https://academic.oup.com/petrology/advance-article/doi/10.1093/petrology/egad022/7115969 by University of Edinburgh user on 18 April 2023